Brain, Behavior, and Immunity xxx (xxxx) xxx

Contents lists available at ScienceDirect

Brain Behavior and Immunity

journal homepage: www.elsevier.com/locate/ybrbi

Neuroimmune mechanisms of cognitive impairment in a mouse model of Gulf War illness

Joshua D. Bryant [a], Maheedhar Kodali [b], Bing Shuai [b], Saeed S. Menissy [a], Paige J. Graves [a], Thien Trong Phan [c], Robert Dantzer [c], Ashok K. Shetty [b], Laura Ciaccia West [a,*], A. Phillip West [a,*]

[a] Department of Microbial Pathogenesis and Immunology, College of Medicine, Texas A&M University Health Science Center, Bryan, TX, USA
[b] Institute for Regenerative Medicine, Department of Molecular and Cellular Medicine, College of Medicine, Texas A&M University Health Science Center, College Station, TX, USA
[c] Department of Symptom Research, Division of Internal Medicine, The University of Texas MD Anderson Cancer Center, Houston, TX, USA

ARTICLE INFO

Keywords:
Gulf War illness
Innate immune signaling
Sex differences
Memory impairment
Neuroinflammation
Mitochondrial dysfunction

ABSTRACT

Gulf War Illness (GWI) is a chronic, multi-symptom disorder affecting approximately 30 percent of the nearly 700,000 Veterans of the 1991 Persian Gulf War. GWI-related chemical (GWIC) exposure promotes immune activation that correlates with cognitive impairment and other symptoms of GWI. However, the molecular mechanisms and signaling pathways linking GWIC to inflammation and neurological symptoms remain unclear. Here we show that acute exposure of murine macrophages to GWIC potentiates innate immune signaling and inflammatory cytokine production. Using an established mouse model of GWI, we report that neurobehavioral changes and neuroinflammation are attenuated in mice lacking the cyclic GMP-AMP synthase (cGAS)-Stimulator of Interferon Genes (STING) and NOD-, LRR- or pyrin domain-containing protein 3 (NLRP3) innate immune pathways. In addition, we report sex differences in response to GWIC, with female mice showing more pronounced cognitive impairment and hippocampal astrocyte hypertrophy. In contrast, male mice display a GWIC-dependent upregulation of proinflammatory cytokines in the plasma that is not present in female mice. Our results indicate that STING and NLRP3 are key mediators of the cognitive impairment and inflammation observed in GWI and provide important new information on sex differences in this model.

1. Introduction

Gulf War illness (GWI) is a chronic, multi-symptom disorder affecting approximately 25 to 32 percent of the nearly 700,000 veterans of the 1991 Persian Gulf War (PGW-1) (White, 2016). The neuropsychiatric features of GWI include learning and memory deficits, depression, and anxiety, and GWI appears to be linked to synergistic exposure to chemicals including the nerve gas prophylactic pyridostigmine bromide (PB), a reversible acetylcholinesterase inhibitor, and permethrin (Per), an insecticide (White, 2016; Golomb, 2008).

Research over the past few decades has uncovered mechanisms by which exposure to GWI-related chemicals (GWIC) causes GWI pathology and symptoms. Studies of veterans with GWI have revealed immune changes, including increases in inflammatory cell types (Zhang, 1999; Johnson et al., 2016; Parkitny et al., 2015), heightened production of proinflammatory cytokines (Zhang, 1999; Broderick, 2011; Broderick, 2013; Janulewicz et al., 2019), and transcriptional profiles that resemble those observed in autoimmune disorders (Craddock et al., 2015). Studies using rodent models of GWI have also demonstrated immune alterations due to GWIC exposure, including increases in proinflammatory cytokines in the hippocampi of GWIC-exposed rats (Shetty et al., 2017) and in the brains and sera of GWIC-exposed mice (Zakirova et al., 2017; Seth et al., 2019). However, the role of the innate immune system in GWI pathology remains uncharacterized, and the signaling cascades responsible for proinflammatory cytokine induction in animal models and veterans with GWI are unknown.

GWIC exposure enhances reactive oxygen species (ROS) production and oxidative stress (White, 2016; Golomb, 2008), which may contribute to a vicious cycle of mitochondrial dysfunction by damaging mitochondrial DNA (mtDNA) and oxidative phosphorylation (OXPHOS)

* Corresponding authors.
E-mail addresses: lwest@tamu.edu (L. Ciaccia West), awest@tamu.edu (A.P. West).

https://doi.org/10.1016/j.bbi.2021.07.015
Received 27 August 2020; Received in revised form 13 July 2021; Accepted 24 July 2021
Available online 29 July 2021

proteins to further augment ROS and trigger progressively increasing mitochondrial stress. Multiple studies have documented mitochondrial dysfunction both in veterans with GWI (Koslik et al., 2014; Golomb, 2014; Chen et al., 2017) and in murine models of GWI (Shetty et al., 2017; Zakirova et al., 2017; Abdullah et al., 2016; Emmerich et al., 2017). Moreover, clinical manifestations of GWI resemble those identified in Chronic Fatigue Syndrome (CFS), a disease linked closely with mitochondrial dysfunction (Golomb, 2014; Castro-Marrero, 2013). In addition, several GWI studies have demonstrated mitochondrial dysfunction and inflammation contemporaneously, suggesting an interaction between these two disease mechanisms (West, 2017). Mitochondria have well-appreciated roles in cellular metabolism and apoptosis, but they are also key immune regulators, impacting many aspects of signaling and effector responses in both the innate and adaptive immune system (West et al., 2011). Mitochondrial dysfunction and mtDNA damage can trigger a wide range of inflammatory responses that have been implicated in immune-mediated pathology (Nakahira et al., 2015).

Based on evidence of mitochondrial dysfunction and inflammation in GWI, and on the documented link between the two, we hypothesized that exposure to GWIC might engage immune pathways known to be important in detecting mitochondrial dysfunction, contributing to inflammatory responses that exacerbate neuropathology and cognitive symptoms of GWI. To test this hypothesis, we used an established mouse model of GWI in which mice are exposed to GWIC by intraperitoneal injection for a period of 10 days, developing cognitive impairment and neuroinflammation beginning at 5 months post-exposure (Ojo, 2014; Zakirova, 2015; Zakirova et al., 2015). In our study, we employed a longitudinal analysis regimen, performing cognitive tests followed by analysis of hippocampal and plasma cytokine expression, hippocampal astrocyte and microglia abundance and morphology, and hippocampal mitochondrial protein expression at the terminal timepoint. We used both female and male mice in these experiments to evaluate sex-dependent effects of GWIC, as there is evidence that GWI can be more severe in women (Heboyan, 2019). To examine the acute effects of GWIC exposure on metabolism and cell-intrinsic immune responses, we performed a series of *in vitro* experiments using bone marrow-derived macrophages (BMDMs). Finally, we applied this GWIC-exposure model to C57BL/6 genetic knockouts lacking key innate immune sensors that interface with mitochondria and cellular metabolism to evaluate the contributions of these inflammatory signaling pathways to the development of GWI pathology. Our results provide important new information on sex differences in GWI-related pathology and reveal that innate immune signaling contributes to cognitive impairment and inflammation in an accepted animal model of GWI.

2. Materials and methods

2.1. Animals, study design, and Gulf War chemical agents

Supplementary Fig. 1A depicts study design. Wild-type (WT) C57BL/6J mice used in these experiments were purchased directly from Jackson Laboratories and allowed to acclimate to the animal facility for 2–4 weeks prior to exposure. NLR Family Pyrin Domain Containing 3 null (NLRP3$^{-/-}$) (JAX strain 021302) and Stimulator of Interferon Genes Goldenticket (STING$^{gt/gt}$) (JAX strain 017537) C57BL/6J mice were bred in-house using breeding pairs purchased from Jackson Laboratories. NLRP3$^{-/-}$ mice are homozygous for a neo cassette in the coding region of *Nlrp3* and are therefore deficient in NLRP3 inflammasome activity (Kovarova, 2012), whereas STING$^{gt/gt}$ mice are homozygous for an I199N missense mutant allele in the *Sting* gene and express no STING protein (Sauer, 2011). Mice were 12 weeks old when exposed to DMSO or GWIC, consistent with published studies (Zakirova et al., 2015). Mice were group-housed in humidity-controlled environments maintained at 22 °C on 12-hour light–dark cycles (600–1800). Food and water were available *ad libitum*.

Mice were randomly assigned to treatment cohorts: DMSO vehicle control (10 mice per sex for WT mice, 6 mice per sex for NLRP3$^{-/-}$ and STING$^{gt/gt}$ mice) or GWIC (10 mice per sex for WT, NLPR3$^{-/-}$, and STING$^{gt/gt}$ mice) (Supplementary Fig. 1A). Mice then underwent an exposure regimen of 10 days of daily peritoneal injections of 50 μl of 100% DMSO alone for DMSO cohorts or 50 μl of GWIC (0.7 mg per kilogram bodyweight of PB and 200 mg per kilogram bodyweight of Per) dissolved in 100% DMSO for GWIC cohorts. Five months after the 10-day exposure, all mice were subjected to neurobehavioral tests as described below. Testing occurred in a room immediately adjacent to the housing room, and mice were acclimated to the testing room and apparatus one day prior to beginning testing. Twelve months after exposure, mice were retested, and then all mice were euthanized for tissue processing or immunohistochemical analysis.

This study was approved by the Texas A&M Animal Care and Use Committee (TAMU IACUC) (Animal Use Protocol (AUP) 2017–0124 D) and by the Animal Care and Use Review Office (ACURO) of the Department of the U.S. Army Medical Research and Development Command (USAMRDC) (Protocol GW160078.01). These AUPs underwent 3-year review/renewal in 2020 by both TAMU IACUC (AUP 2020–0164 D) and USAMRDC ACURO (GW160078.02). The euthanasia methods employed in the study were consistent with the recommendations of the American Veterinary Medical Association (AVMA).

Pyridostigmine bromide (>98% purity) was purchased from Sigma-Aldrich (catalog number P9797) and permethrin (>98% purity) was purchased from MedChemExpress (catalog number HY-B0887).

2.2. Neurobehavioral tests for analyses of cognitive function

2.2.1. Object location test (OLT)

To evaluate GWIC-dependent cognitive impairment, we subjected all mice to an object location test (OLT), which assesses the ability to perceive changes in the environment. The OLT involved three sequential phases (Fig. 1A): first, in the habituation phase, the mouse was placed at the corner of an empty open field apparatus and allowed to freely explore for five minutes. This was followed by the sample phase, in which the mouse was placed in the corner of the same open field apparatus, which now contained two identical objects placed on opposite sides of the box and allowed to free explore for five minutes. In the final testing phase, after an inter-trial interval of 20 min (5 months post-exposure) or 2 h (12 months post-exposure), the mouse was placed in the corner of the open field apparatus, with one of the objects remaining in its original location (designated as the “familiar location”) and the other object moved to a novel location (designated as the “novel location”). The apparatus was cleaned with 70% ethanol and allowed to air-dry prior to the commencement of each trial. Mouse movement in the sample and testing phases was continuously video-tracked using the Noldus Ethovision XT program; the nose-point of the mouse coming within 2 cm of an object was recorded by the software as object exploration. Data on time spent exploring both objects, total distance traveled, and velocity of movement during these phases were collected and are shown in Supplementary Table 1. Data from trials in which mice spent <10 s total exploring both objects in either the sample or test trial were excluded. Percent time with object was calculated as total time exploring the objects in the novel or familiar location, divided by total time exploring both objects. Discrimination index was calculated as total time exploring the object in the novel location subtracted by total time exploring the object in the familiar location, divided by total time exploring both objects. Cohorts were tested at both 5 and 12 months after GWIC exposure, with similar results observed. All data shown is from 5 months post-exposure.

2.2.2. Novel object recognition test (NORT)

In addition to the OLT, we subjected all mice to the novel object recognition test (NORT) in order to assess memory and cognition. The NORT involved three sequential phases (Fig. 1E): an initial habituation

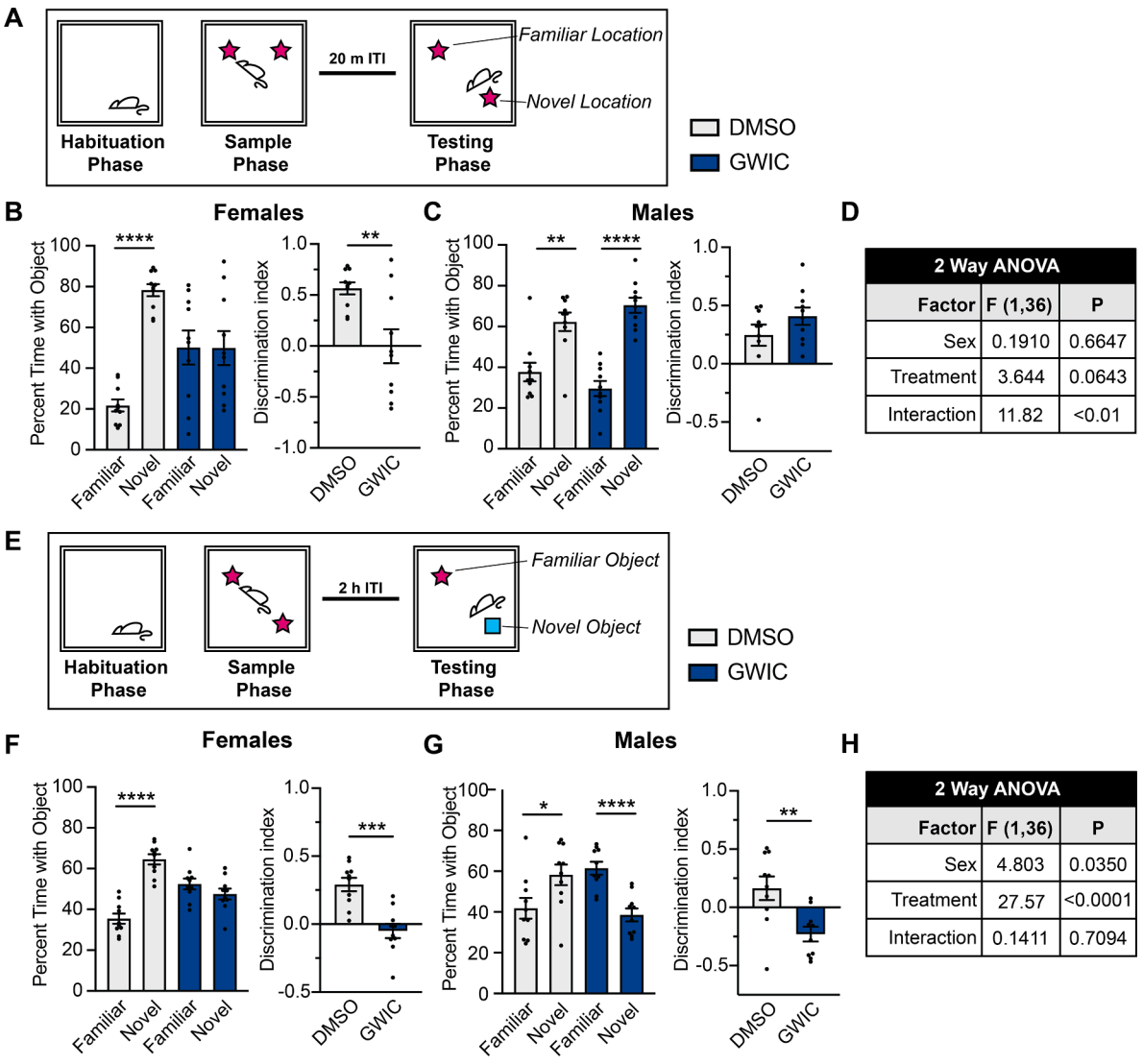

Fig. 1. Exposure of C57BL/6 wild-type mice to GWIC results in sex-dependent impairments in spatial memory and novel object recognition. (A) The sequential phases used in the object location test (OLT): the habituation phase, the sample phase, and the testing phase. Each phase lasted five minutes, and the inter-trial interval (ITI) between the sample and testing phase was 20 min. (B) Percentages of total exploration time spent with the object in the familiar and novel location in the testing phase, and OLT discrimination index as calculated for DMSO- and GWIC-exposed female mice. (C) Percentages of total exploration time spent with the object in the familiar and novel location in the testing phase, and OLT discrimination index as calculated for DMSO- and GWIC-exposed male mice. (D) Two-way ANOVA analysis of sex, treatment, and interaction effect for the OLT. (E) The sequential phases used in the novel object recognition test (NORT): the habituation phase, the sample phase, and the testing phase. Each phase lasted five minutes, and the inter-trial interval (ITI) between the sample and testing phase was 2 h. (F) Percentages of total exploration time spent with the familiar and novel object in the testing phase, and NORT discrimination index as calculated for DMSO- and GWIC-exposed female mice. (G) Percentages of total exploration time spent with the familiar and novel object in the testing phase, and NORT discrimination index as calculated for DMSO- and GWIC-exposed male mice. (H) Two-way ANOVA analysis of sex, treatment, and interaction effect for the NORT. Error bars represent the mean of biological replicates ± SEM (N = 10). Indicated p-values for B, C, F, and G were calculated two-tailed, unpaired, Student's *t*-test. *p < 0.05; **p < 0.01; ***p < 0.001; ****p < 0.0001..

phase as described for the OLT, a second sample phase in which the mouse explored the open field containing two identical objects, and, following an inter-trial interval of 2 h (5 months post-exposure) or 5 h (12 months post-exposure), a testing phase in which one of the original objects was replaced in the same location with a novel object; the unchanged object is designated as the "familiar object." Mice were video-tracked and data was collected as described for the OLT. Percent time with object and discrimination index were calculated as for the OLT. As for the OLT, data from trials in which mice spent <10 s total exploring both objects in either the sample or test trial were excluded. Cohorts were tested at both 5 and 12 months after GWIC exposure, with similar results observed. All data shown is from 5 months post-exposure.

2.2.3. Measurement of weight change and locomotor activity

To assess changes in health and activity following DMSO and GWIC exposure, all mice were weighed prior to the first injection, then reweighed at 14 days and 3 months post-exposure in order to calculate a percent change in weight for each mouse (Supplementary Fig. 1B).

To ensure that GWIC did not interfere with general locomotor activity, an additional, separate cohort of C57BL/6 mice, including both females and males, were individually housed with in-cage, low-profile running wheels connected to an activity counter to allow for assessment of hourly running activity, as described previously (Grossberg, 2020). After stabilization of their wheel running activity for 2 weeks, they were exposed to DMSO or GWIC, as described in Section 2.1, with nine mice total per treatment group. Daily wheel running activity was

continuously recorded for three months following exposure.

2.3. Immunohistochemical methods

To assess GFAP+ and IBA-1+ cells in the brain twelve months after exposure to GWIC, mice were deeply anesthetized using an isoflurane vaporizer, then perfused with 4% paraformaldehyde. Brains were postfixed for 18 h in 4% paraformaldehyde and cryoprotected in 30% sucrose. A cryostat was then used to cut 30 μm thick coronal sections through the entire brain. The sections were collected serially in 24-well plates containing phosphate buffer; sections through the cerebral cortex at hippocampal levels were chosen and processed for immunohistochemical quantification of glial fibrillary acidic protein (GFAP)-positive astrocytes and ionized calcium-binding adaptor molecular 1 (IBA-1)-positive microglia. Briefly, sections were incubated in 20% methanol and 3% hydrogen peroxide in phosphate buffered saline (PBS) for 20 min, rinsed three times in PBS, then incubated for 30 min in PBS containing 0.1% Triton-X 100 and 10% serum (Sigma). Following this, sections were incubated in primary antibody (rabbit anti-GFAP antibody or goat anti-IBA-1 antibody, both from Abcam) for 18–48 h, then biotinylated secondary antibody (biotinylated horse anti-goat IgG or biotinylated goat anti-rabbit IgG from Vector Laboratories) for 60 min, then an avidin/biotin complex reagent (Vectastain Elite ABC HRP Kit) for 60 min, with a triple wash in PBS between each incubation step. The peroxidase reaction was developed using Vector SG HRP substrate (Vector Laboratories), then sections were mounted on gelatin-coated slides, dehydrated, cleared, and coverslipped.

2.4. Analysis of hippocampal inflammation

Hippocampal inflammation was evaluated by analysis of astrocyte hypertrophy, activation of IBA-1+ cells, and hippocampal cytokine expression.

2.4.1. Astrocyte hypertrophy and activated IBA-1+ cells

Astrocyte hypertrophy was evaluated using ImageJ to calculate area fraction of GFAP+ structures in three regions (CA1, CA3, and dentate gyrus (DG)) of the hippocampus in 5–6 mice per genotype per sex, for DMSO- and GWIC-exposed cohorts. Four sections per mouse were imaged at 20× and averaged; image collection and ImageJ analysis were blinded to treatment group. Area fraction was calculated by dividing GFAP+ area by total image area.

Activated IBA-1+ cells in three regions of the hippocampus (CA1, CA3, and DG) were evaluated by performing morphological analysis, as described in Fernández-Arjona et al. (2017). All image collection and morphological analysis was performed by the same individual, who was blinded to treatment group. First, for each brain region (CA1, CA3, and DG), four sections per mouse were imaged at 20X and analyzed for the total number of IBA-1+ cells, determined by counting IBA-1+ structures. The same four images were then analyzed for activated IBA-1+ structures, which were defined as IBA-1+ cells with swollen, ramified cell bodies and short, thick processes (Fernández-Arjona et al., 2017). Percentages of activated IBA-1+ cells were computed as the number of activated IBA-1+ cells divided by the total number of IBA-1+ cells. For each hippocampal region, average percentages of activated IBA-1+ cells were calculated for each mouse as the average of four brain sections, with 5–6 mice per experimental group.

2.4.2. Hippocampal cytokine and chemokine analysis.

Hippocampal cytokines were measured using Proteome Profiler Mouse XL Cytokine Arrays (R&D Systems, ARY028). Hippocampal protein extracts were generated as described in Section 2.6 below. For each array, 50 μg of protein from four separate mice was pooled to give a total of 200 μg protein per array. Arrays were processed according to the manufacturer's instructions. Arrays were developed using X-ray film with multiple exposure times. Each cytokine in the array is represented by a duplicate pair of spots. Cytokine levels were determined by measuring the integrated pixel density of a 10-minute exposure using a semi-automated plugin for ImageJ (Klemm, 2020). Pixel density data was normalized based on the total pixel density of the array. Values within one standard deviation of the mean pixel density of a blank area of film were considered below the detection limit. Fold change was calculated by averaging the normalized pixel density of duplicate spots and comparing expression in GWIC-exposed mice to DMSO-exposed mice (GWIC/DMSO). If only one replicate was above the detection limit, only that value was used for the fold change calculation. Normalized density values for all cytokines are reported in Supplementary Table 2.

2.5. Analysis of plasma cytokines

To assess cytokines in the plasma, blood was collected upon euthanasia by cardiac puncture into heparinized tubes. Blood was centrifuged at 4 °C at 1000 × g for 10 min. The resulting plasma was stored at −80 °C for future analysis. Plasma cytokines were measured using the LEGENDplex Mouse Inflammation Panel (BioLegend, 740446) by following the manufacturer's instructions. LEGENDplex samples were measured using a BD LSR Fortessa X-20 Cell Analyzer (BD Biosciences). Flow cytometry data were analyzed using the LEGENDplex Data Analysis Software Suite (BioLegend).

2.6. Tissue processing and expression analysis

For collection of tissues, animals were euthanized, and brains were quickly removed. The entire hippocampus from both hemispheres was micro-dissected from each brain, then snap frozen on dry ice. Cells and tissues were lysed in 1% NP-40 lysis buffer supplemented with protease inhibitor and then centrifuged at 12,000 × g, 4 °C to obtain cellular lysate. After BCA protein assay (Thermo Fisher Scientific, 23225), equal amounts of protein (10–20 μg) were separated on 10–20% SDS–PAGE gradient gels, then transferred onto PVDF membranes. After air drying to return to a hydrophobic state, membranes were incubated in primary antibodies (Supplementary Table 4) at 4 °C overnight in 1X PBS containing 1% casein and 0.02% sodium azide. After incubating with HRP-conjugated secondary antibody at room temperature for 1 h, membranes were developed with Luminata Crescendo Western HRP Substrate (Millipore). Densitometry was performed in ImageJ and normalized to the α-Tubulin or VDAC expression level as indicated.

2.7. In vitro bone marrow-derived macrophage experiments

To assess a direct effect of GWIC exposure on innate immune signaling, we performed a series of *in vitro* experiments using bone marrow-derived macrophages (BMDMs), which, although not derived from the brain, provide a robust cellular platform to evaluate innate immune responses. BMDMs were generated from bone marrow collected from femurs and tibiae isolated from untreated C57BL/6 WT female and male mice, and differentiated using supernatant from L929 cells, which were obtained from ATCC and maintained in DMEM (Sigma, D5796) supplemented with 10% FBS (VWR, 97068–085). Briefly, legs were dissected from mice and muscle and tissue were removed. Bones were immersed in 70% EtOH then washed with PBS. Bones were crushed with a mortar and pestle and the marrow was collected in DMEM. The marrow was passed through a 70 μm mesh strainer, then blood cells were lysed using ACK lysis buffer. Remaining cells were passed through a 40 μm mesh strainer and plated on Petri dishes in DMEM containing 10% FBS and 30% L929 culture media for a total of 7 days before plating for experiment. At day 4, the media was refreshed with additional DMEM (10% FBS and 30% L929). At day 5, permethrin (10 μM final) and/or pyridostigmine bromide (PB, 100 ng/mL) were added to cells in the GWIC treatment group as indicated, and cells were maintained with the same concentration of GWIC for the remainder of the experiment.

For all experiments, BMDMs were plated on day 7 at a density of 6×10^5 cells/mL, unless otherwise indicated, and allowed to adhere overnight. To examine the direct effects of GWIC exposure on innate immune signaling, we then stimulated the BMDMs with either bacterial lipopolysaccharide using LPS-B5 Ultrapure (InvivoGen, tlrl-pb5lps) at a concentration of 200 ng/mL (unless otherwise indicated) or transfected them with interferon stimulating DNA (ISD) (InvivoGen, tlrl-isdn) into the cytosol using Polyethyleneimine (PEI) (Alfa Aesar, 43896).

2.8. ELISA

To measure cytokine production in BMDMs following innate immune stimulation, ELISAs were performed. Capture and detection antibodies were purchased from BioLegend (Supplementary Table 4). Detached cells and debris were removed from cell culture supernatant by centrifugation prior to the assay. After incubating half-well ELISA plates in capture antibodies at 4 °C overnight, plates were blocked with PBS containing 10% FBS at room temperature for 1 h. Cell culture supernatants were diluted 80-240x (for IL-6) or 2-20x (for TNF-α) in blocking buffer. Standards and cell culture supernatant were added to the ELISA plates and incubated at room temperature for 2 h. Plates were incubated at room temperature with biotin-conjugated detection antibody (1:200) for 1 h, followed by Avidin-HRP (1:1000) and detection with a TMB Substrate Set (BioLegend, 421101). Plates were washed 4 times with PBS containing 0.05% Tween-20 between each step.

2.9. Metabolic analysis

To assess whether acute exposure of BMDMs result in metabolic rewiring, we performed metabolic analyses. The Seahorse XFe96 Analyzer (Agilent) was used to measure mitochondrial respiration and glycolysis simultaneously following a modified protocol. Briefly, BMDMs were isolated and treated with GWIC as described above. At day 7, BMDMs were plated at a density of $6x10^4$ cells/well in 80 μL of culture medium in an Agilent Seahorse XF96 Cell Culture Microplate. After 3 h, an additional 80 μL of medium was added containing permethrin (10 μM final) and/or pyridostigmine bromide (100 ng/mL final) as indicated. After incubating overnight, an additional 40 μL culture medium containing LPS (200 ng/μL final) was added as indicated. Following a 6-hour incubation, cells were washed with PBS and media was replaced with XF assay medium (Base Medium Minimal DMEM lacking glucose, glutamine, and bicarbonate, supplemented with 2 mM Ala-Gln, pH 7.4) prior to analysis. Oxygen consumption rate (OCR) and extracellular acidification rate (ECAR) were measured after sequential addition of glucose 25 mM; oligomycin (1.5 μM); FCCP (1.5 μM) + sodium pyruvate (1 mM); and antimycin A (833 nM) + rotenone (833 nM). Beginning the run with glucose omitted from the medium allows both respiratory and glycolytic parameters to be determined in the same run. Respiratory and glycolytic parameters were calculated using the equations outlined in the Seahorse XF Mito Stress Test and Glycolysis Stress Test manuals.

2.10. Statistical analyses

Outliers were removed using the ROUT algorithm in GraphPad prism with q set to 1%. All p-values were calculated using two-tailed, unpaired, Student's *t*-test; one-way ANOVA; or two-way ANOVA as indicated in figure legends using GraphPad Prism or Excel. *Post hoc* analyses were done with Tukey's multiple comparison or the linear two-stage step-up method in GraphPad Prism as indicated in the figure legends.

3. Results

3.1. GWIC-exposed mice show sex differences in cognitive impairment

To establish GWIC-dependent cognitive impairment in our model, we subjected DMSO- and GWIC-treated female and male C57BL/6 wild-type (WT) mice to an object location test (OLT), which assesses the hippocampal-dependent ability to perceive changes in the environment, and to a novel object recognition test (NORT), which depends primarily upon the integrity of the perirhinal cortex region of the cerebral cortex and partially the hippocampus (Hattiangady, 2014). These tests have been used in rat models of GWI to show cognitive changes in male animals with demonstrated hippocampal inflammation (Hattiangady, 2014; Kodali, 2018; Madhu, 2019; Shetty, 2020), and we sought to expand this analysis to a mouse model of GWI, with the inclusion of female animals.

Notably, female, but not male, GWIC-exposed mice were impaired in the OLT. By measuring time spent with an object in a familiar location and an object in a novel location (Fig. 1A), we were able to calculate a discrimination index (DI, the difference between time spent with the object in the familiar location and time with the object in the novel location divided by the total time spent with both; total object exploration time had to be >10 s for data to be used, and as shown in Supplementary Table 1, averaged between 30 and 100 s for WT mice). DMSO-exposed female mice spent significantly more time ($t = 13.34$, $df = 18$, $p < 0.0001$) with the object in the novel location. This resulted in a mean DI of 0.5650 (Fig. 1B), indicating an ability to perceive object location changes. In contrast, GWIC-exposed female mice spent equivalent time with both objects ($t = 0.02096$, $df = 18$, $p = 0.9834$), resulting in a mean DI of −0.002459, significantly lower ($t = 3.213$, $df = 18$, $p < 0.01$) than the mean DI of the control cohort (Fig. 1B). GWIC-exposed male mice were unimpaired, with both DMSO- and GWIC-exposed male cohorts spending significantly increased time (DMSO, $t = 3.820$, $df = 18$, $p < 0.01$; GWIC, $t = 7.764$, $df = 18$, $p < 0.0001$) with the object in the novel location and showing mean DI values (DMSO, 0.2465; GWIC, 0.4088) that were not significantly different ($t = 1.378$, $df = 18$, $p = 0.1852$) (Fig. 1C). Two-way ANOVA analysis of these data indicate a significant interaction effect of sex and treatment on mean DI [$F(1,36) = 11.82$, $p < 0.01$] (Fig. 1D), supporting observed female sex-dependence on OLT impairment following GWIC exposure. Fig. 1B and 1C depict OLT data from 5-month post-exposure; similar observations were seen at 12 months post-exposure (data not shown).

While only GWIC-exposed female mice were impaired in the OLT, which reflects location memory, GWIC-exposed female and male mice both showed impairment on the NORT, a measure of novel object recognition (Fig. 1E). GWIC-exposed female mice did not spend significantly more time ($t = 1.324$, $df = 18$, $p = 0.2022$) with the novel object, resulting in a mean DI (-0.04982) significantly lower ($t = 4.673$, $df = 18$, $p < 0.001$) than the mean DI of the control cohort (Fig. 1F). Likewise, GWIC-exposed male mice spent significantly less time ($t = 5.155$, $df = 18$, $p < 0.0001$) with the novel object, resulting in a mean DI of −0.2294 that was significantly lower ($t = 3.297$, $df = 18$, $p < 0.01$) than the mean DI of the control male cohort (Fig. 1G). Two-way ANOVA analysis of these data do not demonstrate a significant interaction effect of sex and treatment in mean DI [$F(1,36) = 0.1411$, $p = 0.7094$], but rather show significant effect of treatment due to the impairment observed in both females and males in this test [$F(1.36) = 27.57$, $p < 0.0001$)] (Fig. 1H). Fig. 1F and 1G depict NORT data from 5-months post-exposure, with similar observations seen at 12-months post-exposure (data not shown). These analyses demonstrate that both GWIC-exposed female and male mice were impaired in the NORT.

To rule out the possibility of GWIC-dependent motor deficits that would confound these findings, we collected control data for total distance moved and velocity of movement in the testing phase of the OLT and NORT. Mean distance and velocity did not significantly differ between DMSO- and GWIC-exposed female or male mice at either time post-exposure (5-months post-exposure shown in the blue-shaded portion of Supplementary Table 1; 12-month post-exposure data were similar and are not shown), indicating that GWIC exposure does not result in motor deficits. In addition, DMSO- and GWIC-exposed female and male mice were weighed at both 14 days and 3 months post-

exposure in order to evaluate GWIC-dependent impacts on baseline health and activity. Mean percent weight change did not significantly differ between DMSO- and GWIC-exposed female or male mice at 14 days post exposure (females, $t = 0.5504$, $df = 18$, $p = 0.5888$; males, $t = 0.0.2167$, $df = 18$, $p = 0.9829$) or 3 months post exposure (females, $p = 0.6728$, $t = 0.4293$, $df = 18$; males, $p = 0.9934$, $t = 0.008397$, $df = 18$) (Supplementary Fig. 1B). Finally, wheel running studies were performed to check for possible GWIC-induced impairment in physical activity. DMSO- and GWIC-exposed mice did not display differences in rotations per hour measured on Day 85 post-exposure (Supplementary Fig. 1C), nor did they display differences in the sum of average revolutions per day over the course of three months following exposure ($t = 0.7046$, $df = 17$, $p = 0.4906$) (Supplementary Fig. 1D). These studies therefore indicate that the finding of sex differences in GWIC-dependent cognitive impairment were not confounded by motor deficits resulting from GWIC treatment.

3.2. GWIC-exposed female mice exhibit more pronounced astrocyte hypertrophy and activated microglia in the hippocampus compared to GWIC-exposed male mice

To begin to assess neuroinflammation after GWIC exposure, perfused brains from female and male mice were fixed, sectioned, and processed for immunohistochemical quantification of glial fibrillary acidic protein (GFAP)-positive astrocytes and ionized calcium-binding adaptor molecular 1 (IBA-1)-positive microglia. Analysis of astrocytes in the dentate gyrus (DG), CA1, and CA3 regions of the hippocampus (Fig. 2A, B, and C, respectively) revealed that GWIC-exposed female mice displayed significantly increased GFAP+ structures in all three hippocampal regions as compared to female DMSO-exposed mice (DG, $t = 5.152$, $df = 10$, $p < 0.001$; CA1, $t = 4.798$, $df = 9$, $p < 0.001$; CA3, $t = 6.992$, $df = 9$, $p < 0.0001$). GWIC-exposed male mice showed significantly increased GFAP+ structures in the DG region and CA3 region (Fig. 2D and 2F), but not the CA1 region (Fig. 2E) (DG, $t = 3.446$, $df = 10$, $p < 0.01$; CA1, $t = 1.154$, $df = 10$, $p = 2755$; CA3, $t = 2.937$, $df = 10$, $p < 0.05$). This observation, which indicates more widespread hippocampal astrocyte hypertrophy in GWIC-exposed female mice as compared to GWIC-exposed male mice, is consistent with our finding of sex differences in GWIC-dependent cognitive impairment.

Using this murine GWIC-exposure model, Zakirova and colleagues have likewise observed significant increases of astrocyte hypertrophy in the dentate gyrus of the hippocampus, as measured by GFAP quantification. Notably, this study, which exclusively used male mice, did not observe a significant increase in activated IBA-1+ cells following GWIC-exposure (Zakirova et al., 2015). In contrast, when we performed blinded morphological scoring of IBA-1+ cells within the hippocampi of experimental animals, we observed that GWIC-exposed female mice exhibited a significant increase of IBA-1+ cells with an activated morphology in the DG (Fig. 4C), defined as cells with swollen, ramified cell bodies and short, thick processes (Fernández-Arjona et al., 2017). Significant increases were not observed in the CA1 or CA3 hippocampal regions of GWIC-exposed female (Fig. 4C), and GWIC-exposed male mice displayed a significant reduction in IBA-1+ cells with an activated morphology within the DG and CA1 regions (Supplementary Fig. 6D), consistent with decreases in percent fraction of IBA-1+ cells observed by Zakirova et al. (2015). This suggests microglial cell activation within the DG of female, but not male, GWIC-exposed mice as compared to DMSO controls.

3.3. GWIC-exposed mice show sex differences in cytokine expression

Expanding on our immunohistochemical quantification of GFAP+ and IBA-1+ hippocampal cells, we examined markers of inflammation in the hippocampi of GWIC-exposed mice. Twelve months post-exposure to DMSO or GWIC, mice were euthanized, and hippocampi were microdissected from both hemispheres of the brain. Using Mouse XL cytokine arrays, which provide a semi-quantitative measure of cytokine protein expression, we screened an array of over 100 cytokines and chemokines from hippocampal tissue lysates (Supplementary Table 2). In the hippocampi of GWIC-exposed female mice, we found a profile of cytokine expression that is consistent with neuroinflammation. Several cytokines associated with neuroinflammation were elevated in GWIC-exposed female mice, including pentraxin 3, PCSK9, MMP-2, endostatin, and C-Reactive Protein (CRP) (Supplementary Fig. 2A and B). We further observed a decrease in the immune suppressive cytokines IL-10 and IL-11 as well as the chemokine CCL21.

The overall trend in proinflammatory cytokines differed in GWIC-exposed male mice, which appeared to lack the increases in pentraxin 3, PCSK9, MMP-2, and endostatin observed in GWIC-exposed female mice. However, GWIC-exposed male mice displayed a modest increase in CRP and a decrease in CCL21 similar to female cohorts (Supplementary Fig. 2B), as well as an increase in the proinflammatory cytokine IL-1β, and a decrease in the anti-inflammatory cytokine IL-13 (Supplementary Fig. 2C and D). The anti-inflammatory cytokine IL-4 was increased, as was hepatocyte growth factor (HGF), (Supplementary Fig. 2C and D). We also observed a nearly 4-fold decrease in erythrocyte growth factor (EGF).

In addition to profiling cytokine expression in the hippocampus, we also examined cytokine expression in plasma collected from DMSO or GWIC-exposed mice at 12 months post-exposure. Interestingly, we found that several proinflammatory cytokines were elevated in the plasma of male, but not female, mice. Of the eight cytokines analyzed, none were significantly altered in GWIC-exposed female mice (Fig. 2G). However, in GWIC-exposed male mice, the proinflammatory cytokines IL-23, GM-CSF, MCP-1, and TNF-α were significantly increased, with a trend towards elevation observed in IL-1β (Fig. 2G).

3.4. Exposure of macrophages to GWIC results in increased production of inflammatory cytokines, enhanced expression of interferon-stimulated genes, and metabolic alterations

Although it is appreciated that GWIC exposure causes persistent neuroinflammation, consistent with our *in vivo* findings, a direct effect of GWIC exposure on innate immune signaling has not been documented. To characterize the immediate impact of GWIC on cell-intrinsic innate immune responses, we performed a series of acute, *in vitro* experiments using bone marrow-derived macrophages (BMDMs). While not derived from the brain, BMDMs provide a robust cellular platform to evaluate innate immune responses (Kelly and O'Neill, 2015). BMDMs were first pre-treated for 3 days with permethrin (Per) alone, pyridostigmine bromide (PB) alone, or, as in the *in vivo* experiments, both GWIC (Per-PB). To examine how GWIC exposure modulates innate immune signaling pathways, we then stimulated the BMDMs with bacterial lipopolysaccharide (LPS), an agonist of the innate immune sensor Toll-like receptor 4 (TLR4), or transfected them with interferon stimulatory DNA (ISD), which signals through the cGAS-STING pathway (Roers et al., 2016; Chen et al., 2016; Barber, 2015).

ELISA analysis of LPS-treated BMDMs revealed that GWIC exposure synergized with LPS stimulation and resulted in increased proinflammatory cytokine production. Analysis by one-way ANOVA showed that GWIC treatment significantly enhanced IL-6 production after 6 h ($F(3, 36) = 6.835$, $p < 0.001$) and 24 h ($F(3, 36) = 3.772$, $p < 0.05$) (Fig. 3A) and TNF-α production ($F(3, 36) = 5.098$, $p < 0.01$) (Fig. 3B) after 24 h of LPS exposure. *Post hoc* pairwise comparisons showed that Per or Per-PB treatment led to increased production of IL-6 after 6 h and both IL-6 and TNF-α after 24 h of LPS treatment (Fig. 3A and B). Interestingly, though PB alone had no effect on IL-6 and TNF-α production, it appeared to act synergistically with Per and enhanced IL-6 and TNF-α production over Per treatment alone, though the difference between Per and Per-PB treatment groups did not reach statistical significance.

Prior work has shown that systemic LPS-induced TLR4 activation contributes to GWIC-related neuroinflammation (Alhasson et al., 2017;

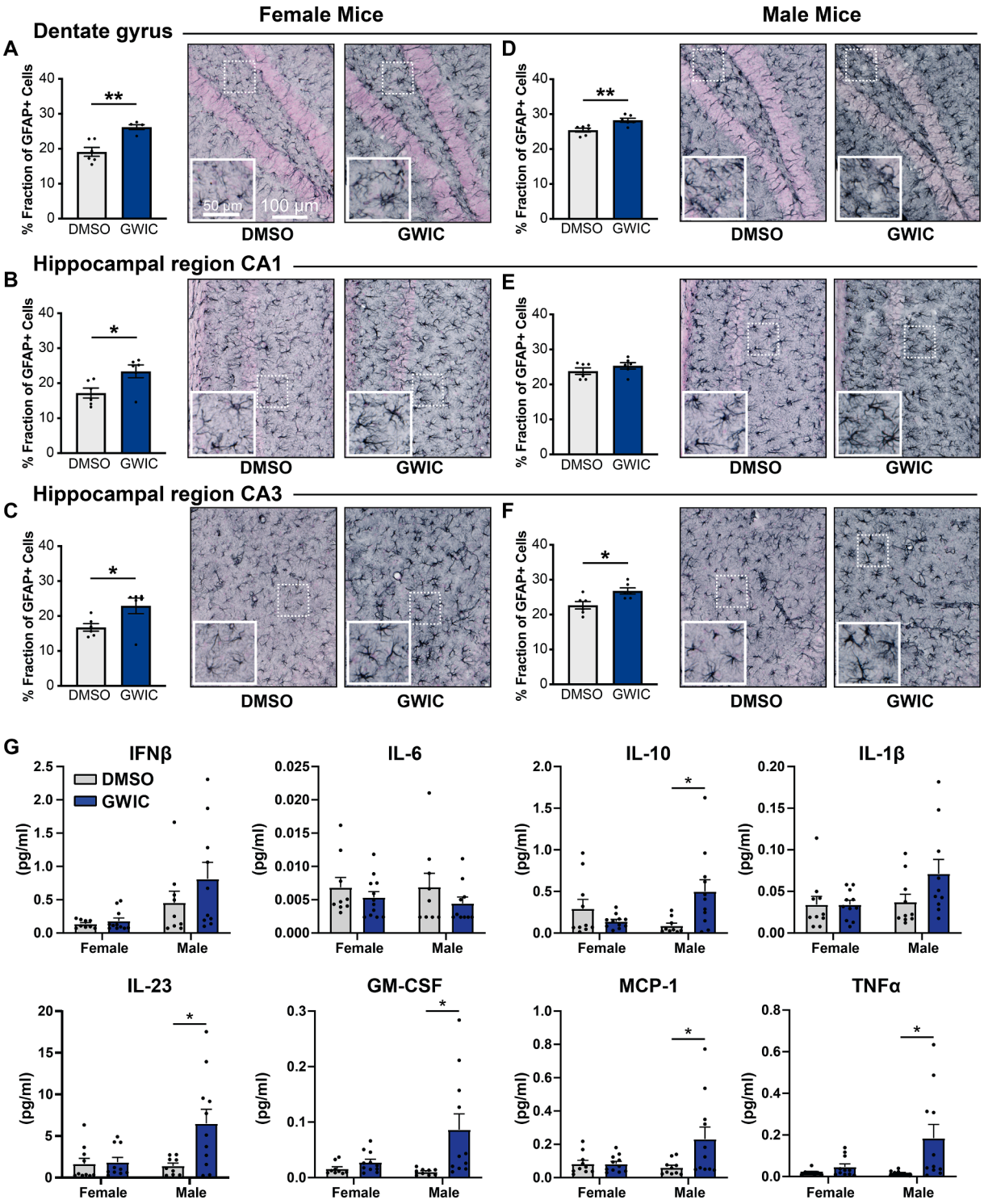

Fig. 2. GWIC exposure results in increased hippocampal astrocyte hypertrophy and increased plasma inflammatory cytokines. We measured percent fraction of glial-fibrillary acidic protein-expressing (GFAP+) cells within the hippocampi of DMSO- and GWIC-exposed female (panels A-C) and male (panels D-F) mice. Three regions of the hippocampus were analyzed: the dentate gyrus (DG) (panels A and D), CA1 (panels B and E), and CA3 (panels C and F). Images show representative distribution and morphology of GFAP+ astrocytes in these three regions in female and male DMSO- and GWIC-exposed mice (scale bar = 100 μM). Insets show magnified views (scale bar = 50 μM); adjacent bar graphs show quantification of percent fraction GFAP+ cells for each cohort, with percent fraction GFAP+ cells calculated as GFAP+ area divided by total image area. Error bars represent the mean of biological replicates ± SEM (N = 5–6). Indicated p-values for A-F were calculated using two-tailed, unpaired, Student's *t*-test. *$p < 0.05$; **$p < 0.01$. (G) Peripheral cytokines measured in plasma collected from DMSO- and GWIC-exposed female and male mice at 12 months post-exposure. Bars represent the mean concentration of biological replicates ± SEM (N = 10 per group). Indicated p-values were calculated using a two-tailed, unpaired, Student's *t*-test. *$p < 0.05$.

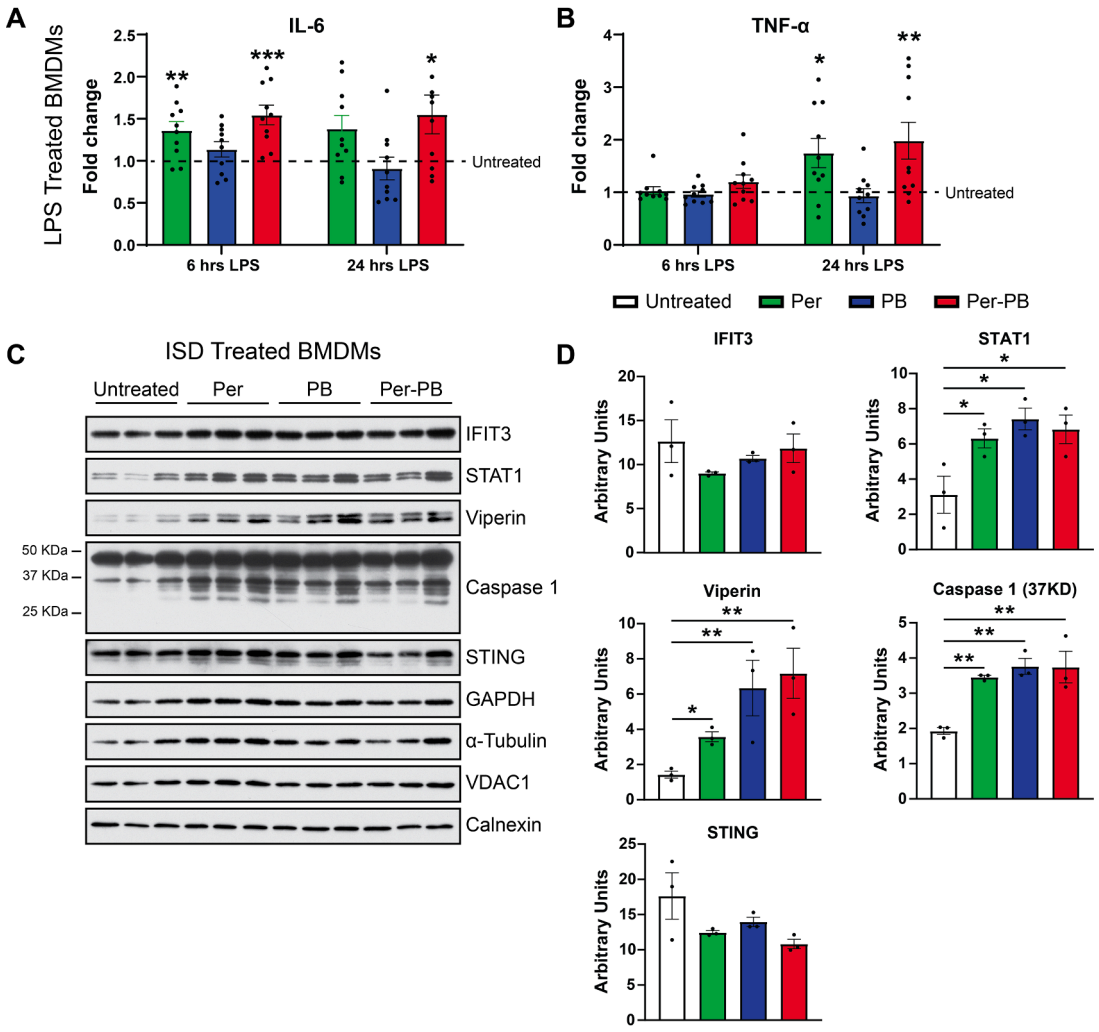

Fig. 3. Acute GWIC exposure potentiates inflammatory responses in BMDMs. ELISA of IL-6 (A) and TNF-α (B) produced by BMDMs treated for 3 days with GWICs as indicated, then treated with 200 ng/mL LPS for 6 or 24 h. Bars represent the mean fold change ± SEM of N = 10 independent experiments in which the cytokine concentration of the LPS-exposed, GWIC-untreated control for each experiment was set to 1. (C) Western blot analysis of ISG expression in BMDMs treated for 3 days with GWICs, then treated with immunostimulatory DNA (ISD) for 24 h. (D) Densitometry of protein expression in (C). Densitometry for each protein was performed in ImageJ and normalized to the α-Tubulin expression level. Bars represent the mean ± SEM for N = 3 biological replicates. Significance values for *post hoc* pairwise comparisons after one-way ANOVA were calculated using the two-stage step-up method to yield q values that have been corrected for the false discovery rate. * $q < 0.05$; ** $q < 0.01$; *** $q < 0.001$.

Bose et al., 2020), and results from our experiments in which GWIC-exposed BMDMs were treated with LPS are consistent with these findings. Similar experiments in which GWIC-exposed BMDMs were transfected with ISD revealed synergy between GWIC-exposure and the cGAS-STING pathway, as GWIC exposure resulted in significantly increased protein expression of the interferon-stimulated genes (ISGs) STAT1 ($F(3,8) = 6.112$, $p < 0.05$) and Viperin ($F(3,8) = 5.969$, $p < 0.0.05$) (Fig. 3C and D). This indicates that signaling downstream of TLR4 and cGAS-STING is enhanced by GWIC treatment and suggests that innate immune system activation may contribute to GWI.

In addition to assessing innate immune responses following acute GWIC exposure, we used this BMDM treatment model to evaluate GWIC-dependent changes in metabolic pathways that affect macrophage activation. BMDMs were again pre-treated with GWIC followed by stimulation with LPS for 6 h, then subjected to analysis of mitochondrial respiration and glycolysis using a Seahorse XF96 Analyzer. GWIC-exposed BMDMs exhibited significantly increased basal mitochondrial oxygen consumption (OCR) ($F(3,16) = 13.12$, $p < 0.001$) and maximal respiration ($F(3,16) = 9.961$, $p < 0.01$) along with a significant increase in proton leak ($F(3,16) = 9.951$, $p < 0.01$) (Supplementary Fig. 3A). LPS treatment completely ablated spare respiratory capacity in all treatment groups. Additional studies analyzing a surrogate marker of glycolysis, the extracellular acidification rate (ECAR), revealed that while glycolysis was largely unchanged following GWIC-exposure alone (not shown), treatment with GWIC plus LPS resulted in cells becoming more glycolytic (Supplementary Fig. 3B), with significant increases to glycolysis ($F(3,16) = 4.849$, $p < 0.05$), glycolytic capacity ($F(3,16) = 25.28$, $p < 0.0001$), and glycolytic reserve ($F(3,16) = 28.79$, $p < 0.0001$), consistent with the immunometabolic changes typically seen in inflammatory M1 macrophages (Freemerman, 2014).

Having found evidence of metabolic rewiring after acute exposure to GWIC, we next investigated whether these changes could persist long after the initial GWIC exposure. Following completion of behavioral tests at 12 months, brains were microdissected to isolate the hippocampus, and protein extracts were generated and subjected to Western blotting and densitometry quantification. Examination of several mitochondrial proteins revealed widespread rewiring of mitochondrial protein expression in the hippocampi of GWIC-exposed mice, particularly enzymes involved in oxidative phosphorylation complexes I-V (OXPHOS CI-CV). Interestingly, the expression of several OXPHOS proteins was

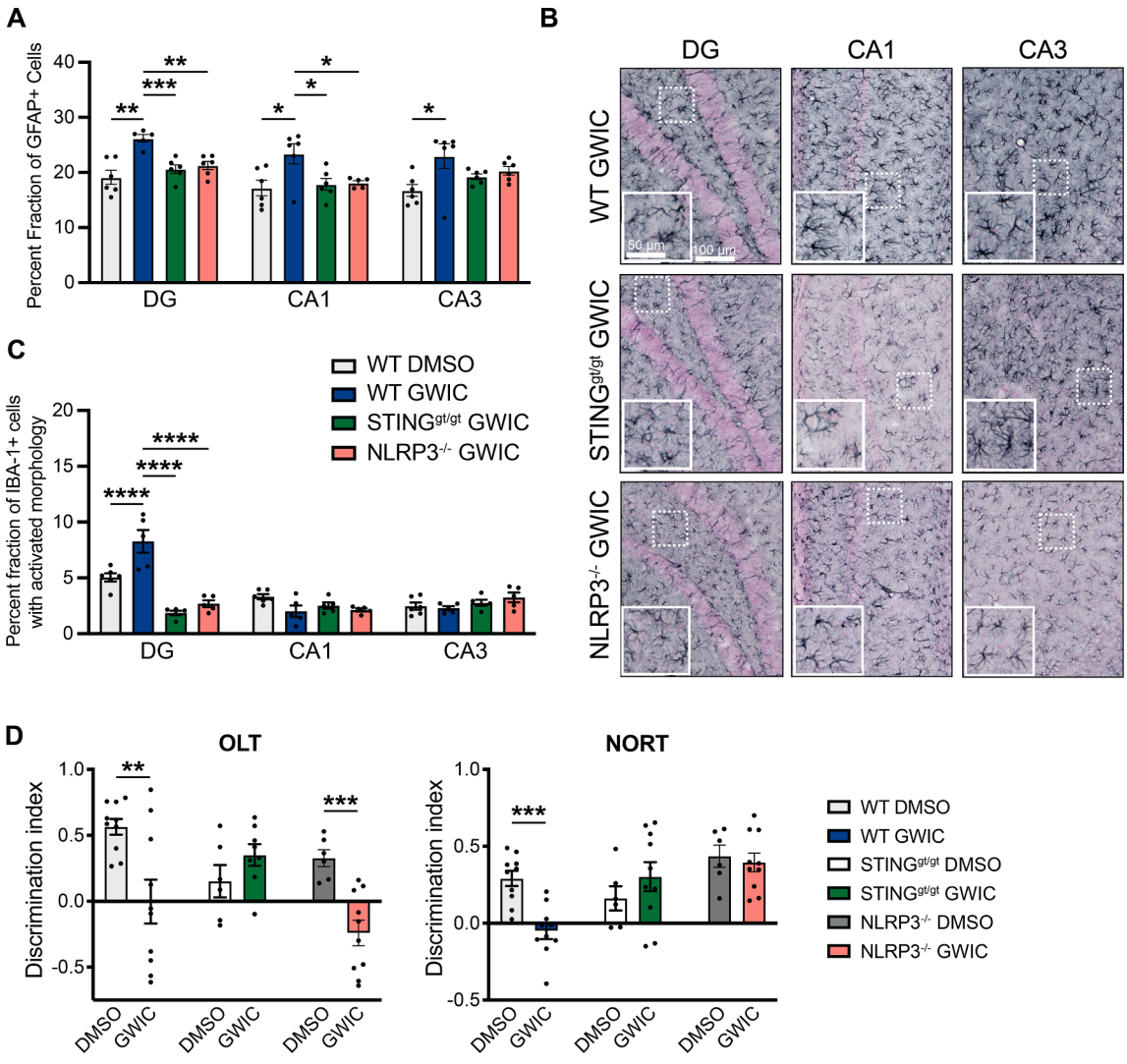

Fig. 4. Loss of STING or NLRP3 attenuates GWIC-related inflammation and cognitive impairment. (A) Comparison of percent fraction of GFAP+ cells within the dentate gyrus (DG), CA1, and CA3 of WT DMSO- or GWIC-exposed female mice and STING$^{gt/gt}$ and NLRP3$^{-/-}$ GWIC-exposed female mice. Error bars represent the mean of biological replicates ± SEM (N = 6). (B) Images show representative distribution and morphology of GFAP+ astrocytes in these three regions in WT, STING$^{gt/gt}$, and NLRP3$^{-/-}$ GWIC-exposed female mice (scale bar = 100 μM). Insets show magnified views (scale bar = 50 μM). (C) Quantification of the percentage IBA-1+ cells with an activated morphology in three hippocampal regions (CA1, CA3, and DG) in WT DMSO- and GWIC-exposed and NLRP3$^{-/-}$ and STING$^{gt/gt}$ GWIC-exposed female mice. Sections were scored blindly for total number of IBA-1+ cells and number of IBA-1+ cells with activated morphology, defined as cells with swollen, ramified cell bodies and short, thick processes (Fernández-Arjona et al., 2017); these values were then used to calculate percent fraction of IBA-1+ cells with activated morphology (number of IBA-1+ cells with activated morphology divided by total number of IBA-1+ cells). (D) Discrimination index of total exploration time spent between the familiar and novel object in the OLT and NORT for STING$^{gt/gt}$ and NLRP3$^{-/-}$ DMSO- and GWIC-exposed female mice. Error bars represent the mean of biological replicates ± SEM (N = 10 for WT DMSO- and GWIC-exposed mice, N = 6 for STING$^{gt/gt}$ DMSO-exposed mice and N = 8–10 for STING$^{gt/gt}$ GWIC-exposed mice, and N = 6 for NLRP3$^{-/-}$ DMSO-exposed mice and N = 10 for NLRP3$^{-/-}$ GWIC-exposed mice). (A, C, D) Indicated p-values were calculated two-tailed, unpaired, Student's *t*-test. *p < 0.05; **p < 0.01; ***p < 0.001; ****p < 0.0001.

significantly increased (NDUFB8 and MT-COI) or decreased (SDHB and ATP5A) in the hippocampi of GWIC-exposed female mice (Supplementary Fig. 3C) but was largely unchanged in the hippocampi of GWIC-exposed male mice, with the exception of a significant decrease in MT-COI (Supplementary Fig. 3D). Overall, our results reveal that GWIC potentiate inflammatory responses to innate immune stimulation and induce immunometabolic rewiring of OXPHOS and glycolysis *in vitro*. Moreover, we observed *in vivo* changes in mitochondrial and metabolic protein expression persisting many months after GWIC exposure, with the most profound alterations occurring in the brains of female mice.

3.5. Ablation of STING or NLRP3 signaling improves cognitive deficits and neuroinflammation following GWIC exposure

Our *in vitro* BMDM experiments revealed synergy between cGAS-STING signaling and GWIC exposure (Fig. 3C and 3D). We also observed a trend towards elevated IL-1β in the plasma of GWIC-exposed male mice (Fig. 2G), as well as a significant increase in caspase 1 following transfection of GWIC-exposed BMDMs with ISD (Fig. 3D), suggesting that GWIC may engage the NLRP3 inflammasome pathway as well. Both STING and NLRP3 are key innate immune pathways triggering inflammation downstream of mitochondrial dysfunction. To interrogate more directly the contribution of STING and NLRP3 signaling to neurobehavioral changes and neuroinflammation following GWIC exposure, cohorts of STING$^{gt/gt}$ and NLRP3$^{-/-}$ mice on a C57BL/6

background were exposed to DMSO or GWIC identically to wild-type C57BL/6 (WT) mice (Supplementary Fig. 1A).

We found that ablation of STING or NLRP3 resulted in changes to the inflammatory profile of GWIC-exposed female mice. As compared to WT cohorts, we observed a trend towards a decrease in pentraxin 3 induction in the hippocampi of STING$^{gt/gt}$ GWIC-exposed female mice, and, unexpectedly, a trending increase in PCSK9 and MMP-2 (Supplementary Fig. 2A and B). In the hippocampi of NLRP3$^{-/-}$ GWIC-exposed female mice, we observed trends toward decreased pentraxin 3, PCSK9, and MMP-2 as compared to WT cohorts (Supplementary Fig. 2C and D). In both STING$^{gt/gt}$ and NLRP3$^{-/-}$ female mice, we observed a trending increase in hippocampal expression of the anti-inflammatory cytokine IL-10 (Supplementary Fig. 2A and B). As with the WT mice, none of the eight plasma cytokines in STING$^{gt/gt}$ and NLRP3$^{-/-}$ GWIC-exposed female mice were significantly elevated above DMSO-exposed cohorts (Supplementary Fig. 4A, Supplementary Fig. 5A).

In male mice, STING ablation resulted in a moderate reduction in HGF expression, although IL-1β remained elevated (Supplementary Fig. 2C and D). As expected, IL-1β was undetectable in NLRP3$^{-/-}$ mice, and the expression of HGF and IL-4 was indistinguishable between DMSO- and GWIC-exposed mice. Interestingly, we observed a trending increase in expression of EGF in NLRP3$^{-/-}$ GWIC-exposed mice (Supplementary Fig. 2C and D). Analysis of plasma cytokines showed that the cytokines significantly increased in WT GWIC-exposed male mice (IL-10, IL-23, GM-CSF, MCP-1, and TNF-α) or trending upwards (IL-1β) were no longer significantly elevated in STING$^{gt/gt}$ and NLRP3$^{-/-}$ GWIC-exposed male mice (Supplementary Fig. 4B, Supplementary Fig. 5B).

The percent fraction of GFAP+ cells in the DG and CA1 hippocampal regions of brains from STING$^{gt/gt}$ and NLRP3$^{-/-}$ GWIC-exposed female mice was significantly lower (DG STING$^{gt/gt}$: $t = 5.221$, $df = 9$, $p < 0.001$; DG NLRP3$^{-/-}$: $t = 4.735$, $df = 9$, $p < 0.01$; CA1 STING$^{gt/gt}$: $t = 2.623$, $df = 10$, $p < 0.05$; CA1 NLRP3$^{-/-}$: $t = 2.568$, $df = 9$, $p < 0.05$; CA3 STING$^{gt/gt}$: $t = 1.614$, $df = 10$, $p = 0.1377$; CA3 NLRP3$^{-/-}$: $t = 1.104$, $df = 10$, $p = 0.2956$) than those observed in WT GWIC-exposed female mice (Fig. 4A and 4B), even though expression of GFAP in the hippocampi of DMSO-treated WT, STING$^{gt/gt}$, and NLRP3$^{-/-}$ was comparable (Supplementary Fig. 6C). This suggests that this is due to lessened GWIC-induced astrocyte hypertrophy in the absence of STING or NLRP3. Analysis of hippocampi from STING$^{gt/gt}$ and NLRP3$^{-/-}$ GWIC-exposed male mice yielded similar observations (Supplementary Fig. 6A and B). In addition, the increase in IBA-1+ cells with activated morphology observed in the DG region of hippocampi from WT GWIC-exposed female mice is ablated in STING$^{gt/gt}$ and NLRP3$^{-/-}$ GWIC-exposed female mice (Fig. 4C), suggesting that these signaling pathways may contribute to the increase in activated IBA-1+ cells in the DG that we observed in our model.

As STING$^{gt/gt}$ and NLRP3$^{-/-}$ GWIC-exposed mice displayed changes in cytokine expression and reduced neuroinflammation, we expected to observe decreased GWIC-dependent cognitive impairment in these mice. Indeed, STING$^{gt/gt}$ GWIC-exposed female mice were unimpaired in the OLT and NORT, in contrast to WT female cohorts, with discrimination indices for DMSO- and GWIC-exposed mice failing to differ significantly for either test (OLT: $t = 1.405$, $df = 12$, $p = 0.1855$; NORT: $t = 1.024$, $df = 14$, $p = 0.3234$) (Fig. 4D, Supplementary Table 3). In contrast, NLRP3$^{-/-}$ GWIC-exposed female mice were unimpaired in the NORT ($t = 0.4192$, $df = 14$, $p = 0.6815$), but still impaired in the OLT ($t = 4.169$, $df = 14$, $p < 0.001$) (Fig. 4D, Supplementary Table 3). As with WT GWIC-exposed male mice, STING$^{gt/gt}$ GWIC-exposed male mice were unimpaired in the OLT ($t = 0.6143$, $df = 8$, $p = 0.5561$), although a decreased N due to low object exploration time by several mice makes conclusions difficult. Likewise, NORT studies using STING$^{gt/gt}$ male mice were inconclusive, as both DMSO- and GWIC-exposed mice failed to spend significantly more time with the novel object in these tests. Studies with NLRP3$^{-/-}$ mice showed that NLRP3$^{-/-}$ GWIC-exposed male mice were unimpaired in the OLT like WT cohorts ($t = 0.2316$, $df = 12$, $p = 0.8208$) and that NLRP3 ablation rescued GWIC-exposed male mice from impairment in the NORT ($t = 2.069$, $df = 14$, $p = 0.0575$) (Supplementary Table 3). Control data for all behavioral tests using STING$^{gt/gt}$ and NLRP3$^{-/-}$ mice are in Supplementary Table 1.

4. Discussion

Using an established murine model of GWI (Ojo, 2014; Zakirova, 2015; Zakirova et al., 2015), we show that GWIC exposure results in sex differences in cognitive impairment, hippocampal astrocyte hypertrophy and activation of IBA-1+ cells, alterations in the levels of hippocampal and plasma cytokines, and changes in the expression of mitochondrial proteins. Assessment of cognitive impairment revealed that GWIC-exposed female mice display impaired object location memory and novel object recognition (Fig. 1B and F), while GWIC-exposed male mice show impairment in novel object recognition only (Fig. 1C and G). These results reveal a significant effect of sex on GWIC-dependent cognitive impairment (Fig. 1D and H) and indicate that females may display more pronounced impairment. A previous study examining both female and male C57BL/6 mice demonstrated increased GWIC-dependent anxiety in female mice, as measured by the open field test (OFT) (Abdullah, 2012). However, the majority of GWI rodent model studies have focused on male mice only, using tests including the Barnes maze (Abdullah et al., 2016; Zakirova, 2015; Zakirova et al., 2015; Joshi, 2018), forced swim test (Joshi, 2018; Joshi et al., 2020), and OFT (Zakirova, 2015; Abdullah, 2012; Abdullah, 2011) to reveal cognitive impairment and depression- and anxiety-related behavior. We tested both GWIC-exposed female and male mice using the OLT and NORT, which have been used in GWI rat models to show impairment in male animals with demonstrated hippocampal inflammation (Hattiangady, 2014; Kodali, 2018; Madhu, 2019; Shetty, 2020). This study is therefore the first time GWIC-exposed female mice have been shown to have cognitive impairment using the OLT and NORT.

In addition to cognitive impairment, we observed astrocyte hypertrophy within all three examined regions (DG, CA1, and CA3) of the hippocampi of GWIC-exposed female mice (Fig. 2A–C), as compared to only two regions (DG and CA3, but not CA1) in male mice (Fig. 2D–F). Comparison of DMSO-exposed female and male mice revealed that control males appear to have heightened astrocyte hypertrophy as compared to control females, which may explain the diminished GWIC-dependent increase. We also observed an increase in IBA-1+ cells with an activated morphology in the DG of GWIC-exposed female mice, suggesting microgliosis (Fig. 4C). This contrasts with the decrease seen in GWIC-exposed male mice (Supplementary Fig. 6D), an observation consistent with a previous study using males only (Zakirova, 2015). Overall, this observation of more pronounced hippocampal astrocyte hypertrophy and activation of IBA-1+ cells observed in GWIC-exposed female mice emphasizes the value of considering both female and male mice for future GWI study.

Sex differences were also observed upon analysis of plasma cytokines. While none of the eight cytokines we examined were increased in the plasma of GWIC-exposed female mice, we observed significantly elevated proinflammatory cytokines IL-23, GM-CSF, MCP-1, and TNF-α, as well as a trend toward elevated IL-1β in the plasma of GWIC-exposed male mice (Fig. 2G). This indicates an intriguing sex-dependent difference in systemic responses to GWIC-exposure: female mice show more pronounced hippocampal astrocyte hypertrophy, activation of IBA-1+ cells, and cognitive impairment, while male mice show increased proinflammatory cytokines in the periphery, associated with mitigated astrocyte hypertrophy and cognitive impairment.

Analysis of cytokines in the hippocampi of GWIC-exposed female and male mice identified interesting inflammatory profiles after GWIC exposure. Analysis of GWIC-exposed female mice revealed a largely proinflammatory cytokine profile, with increases in cytokines associated with inflammation and neuronal cell death including CRP, pentraxin 3, PCSK9, MMP-2, and endostatin. (Supplementary Fig. 2A and B). CRP is commonly measured in the blood as an indicator of systemic

inflammation (Di Napoli, 2011), and CRP expression positively correlates with GWI severity in veterans (Butterick et al., 2019; James et al., 2019). Although CRP is predominantly produced in the liver (Di Napoli, 2011), it is also produced by central nervous system (CNS)-resident cells such as neurons, astrocytes, and microglia (Yasojima et al., 2000; Wight, 2012; Juma, 2011), and increases in the CNS in response to neuroinflammation (Malla et al., 2013). Pentraxin 3 and endostatin are secreted by astrocytes and have been identified as biomarkers of brain injury severity (Shindo et al., 2016; Jeon et al., 2010; Ryu et al., 2012; Malik et al., 2020; Chen et al., 2013; Zhang et al., 2020). PCSK9 is a driver of neuronal inflammation and mediates neuronal cell death by apoptosis (Bingham, 2006; Apaijai, 2019). MMP-2 is often elevated after injury to the brain, such as after ischemia (Planas et al., 2001), and can reduce the integrity of the blood brain barrier (Yin, 2019; Goasdoue et al., 2019; Ni et al., 2018). In addition, we observed a decrease in the expression of the cytokines IL-10 and IL-11, both of which have immune suppressive roles in the brain (Zhang et al., 2020; Zhang, 2019). Finally, consistent with our findings that GWIC-exposed female mice show impaired hippocampal function as measured by the OLT, we observed a decrease in CCL21, which contributes to neurogenesis and memory formation in mice (Turbic et al., 2011). GWIC-exposed male mice displayed a different pattern. Hippocampal analysis demonstrated an increase in CRP and the inflammatory cytokine IL-1β, as well as decreases in anti-inflammatory IL-13 and neurogenerative cytokine CCL21. However, male mice also displayed increases in anti-inflammatory IL-4 and neuroprotective HGF (Benkhoucha, 2010; Kato, 2012; Niimura, 2006), in addition to a decrease in EGF, which modulates the differentiation of neuronal precursors and regulates post-mitotic neurons (Cameron et al., 1998; Wong and Guillaud, 2004; Yamada et al., 1997) (Supplementary Fig. 2C and D).

An important caveat of these analyses is that the cytokine/chemokine blot arrays used to generate these data required significant amounts of protein. We therefore pooled hippocampal lysates from four mice per genotype and condition. This approach that does not allow statistical analysis of the fold change values depicted in Supplementary Fig. 2B and D, thus precluding comparison between experimental cohorts. To draw more definitive conclusions on sex-dependent changes in hippocampal cytokine expression due to GWIC exposure, future studies including more animals and more quantitative techniques are required. However, overall trends observed in these data indicate that GWIC-dependent changes in cytokine expression vary in female and male hippocampi, supported by statistical analysis of plasma cytokines in GWIC-exposed female and male mice.

Our findings strongly emphasize the need to consider sex differences in studies of GWI. While women represented a relatively small percentage (7%) of the active duty population during PGW-1 (Patten and Parker, 2011), chronic GWI conditions differ in female and male PGW-1 veterans (Zundel et al., 2019), with some studies showing female veterans of PGW-1 as more likely to meet the clinical criteria of GWI and to display heightened, longer-lasting GWI symptoms than male veterans (Pierce, 2005; Coughlin, 2017). These sex differences could be caused by multiple factors, including the impact of sex hormones on pathophysiology and disease manifestation (Mauvais-Jarvis et al., 2020), and sex differences in immune responses (Klein and Flanagan, 2016). However, these factors and their contribution to disease are unclear for GWI, establishing a critical need to better understand sex differences in GWI pathology. Our observations of GWIC-exposed female and male mice make a strong argument for the inclusion of both sexes in future preclinical GWI studies involving rodents, as further study is needed to parse sex differences in responses to GWIC.

In addition to inclusion of female and male mice in *in vivo* GWI studies to explore sex differences, we also sought to characterize the immediate impact of GWIC on cells through *in vitro* studies. LPS treatment of BMDMs revealed that GWIC exposure synergizes with LPS to enhance IL-6 and TNF-α production (Fig. 3A and B), supporting previous findings that alterations to the microbiome due to GWIC exposure engages TLR4 to drive inflammation and GWI pathology (Seth et al., 2019; Alhasson et al., 2017; Bose et al., 2020). In addition, GWIC-exposed BMDMs transfected with ISD, which signals through the cGAS-STING pathway, showed heightened production of the interferon-stimulated genes STAT1 and Viperin, as well as an increase in caspase 1, a key component of the NLRP3 inflammasome (Fig. 3C and 3D). As both the cGAS-STING and NLRP3 signaling pathways are downstream of mitochondrial dysfunction and are key signaling pathways in the response to mtDAMPs, these findings raise that possibility that GWIC-dependent mitochondrial dysfunction and mtDAMP production contributes to inflammation during GWI.

Mitochondrial dysfunction (Koslik et al., 2014) and mtDNA lesions (Chen et al., 2017) have been documented in veterans with GWI, and animal studies analyzing expression of nuclear and mitochondrially encoded OXPHOS proteins from whole brain extracts have demonstrated widespread expression changes in mice (Zakirova et al., 2017) and rats (Shetty et al., 2017). We observed sex differences in expression of OXPHOS proteins in hippocampi from GWIC-exposed mice, with females showing significant changes in the abundance of four OXPHOS proteins that were unchanged in male mice (Supplementary Fig. 3C and D). Moreover, we noted decreased expression of manganese superoxide dismutase (MnSOD) and transcription factor A mitochondrial (TFAM) in the hippocampi of female GWIC-treated mice, which play important roles in oxidative stress resistance and mitochondrial DNA homeostasis, respectively. Accordingly, *in vitro* studies of GWIC-exposed BMDMs showed metabolic changes, including a shift to glycolysis similar to that seen in inflammatory M1 macrophages (Freemerman, 2014) (Supplementary Fig. 3A and B). These GWIC-induced mitochondrial changes may result in release of mtDAMPs that could engage innate immune signaling pathways, contributing to GWI-related inflammatory pathology.

To explore this, we conducted GWIC-exposure studies with $STING^{gt/gt}$ and $NLRP3^{-/-}$ mice, which lack the cGAS-STING and NLRP3 signaling nodes that lie downstream of mitochondrial dysfunction (Chen et al., 2016; Gao et al., 2013; Elliott and Sutterwala, 2015; Man and Kanneganti, 2016). Loss of STING or NLRP3 resulted in changes to the cytokine profile observed in the hippocampi of female mice after GWIC exposure (Supplementary Fig. 2A and B), although we are unable to draw statistical conclusions from these data. However, STING and NLRP3 deficient male cohorts did exhibit reduced serum proinflammatory cytokine profiles compared to GWIC-exposed WT mice (Supplementary Fig. 4B and Supplementary Fig. 5B). In addition, both $STING^{gt/gt}$ and $NLRP3^{-/-}$ female and male mice showed a reduction in astrocyte hypertrophy in the hippocampus after GWIC exposure (Fig. 4A and 4B and Supplementary Fig. 6A and B). Moreover, the microglial activation observed in the DG region of GWIC-exposed hippocampi was also absent in $STING^{gt/gt}$ and $NLRP3^{-/-}$ female mice (Fig. 4C), accompanied by improvement on cognitive tests. $STING^{gt/gt}$ GWIC-exposed female mice were successful at both the OLT and NORT, while $NLRP3^{-/-}$ female mice were able to complete the NORT, indicating that both pathways contribute to GWIC-dependent cognitive changes, with potentially a greater role for STING (Fig. 4D) that is consistent with its ability to both engage interferon signaling and activate NLRP3 (Li, 2019).

We have developed a model (Fig. 5), based on our findings and other published studies, that summarizes the proposed mechanisms by which GWIC exposure results in inflammation and cognitive impairment. Our data indicate that exposure to GWIC engages STING and NLRP3 signaling pathways, which contribute to a proinflammatory cytokine profile, astrocyte hypertrophy, and activated IBA-1+ cells in the hippocampi of female mice and astrocyte hypertrophy and elevated proinflammatory cytokines in the plasma of male mice. STING and NLRP3 also appear to contribute to impairments in location memory in female mice and novel object recognition in both female and male mice. STING and NLRP3 signaling pathways represent two of the main mtDAMP sensing pathways, yet it remains unclear what engages these pathways following GWIC-exposure. We hypothesize that mitochondrial

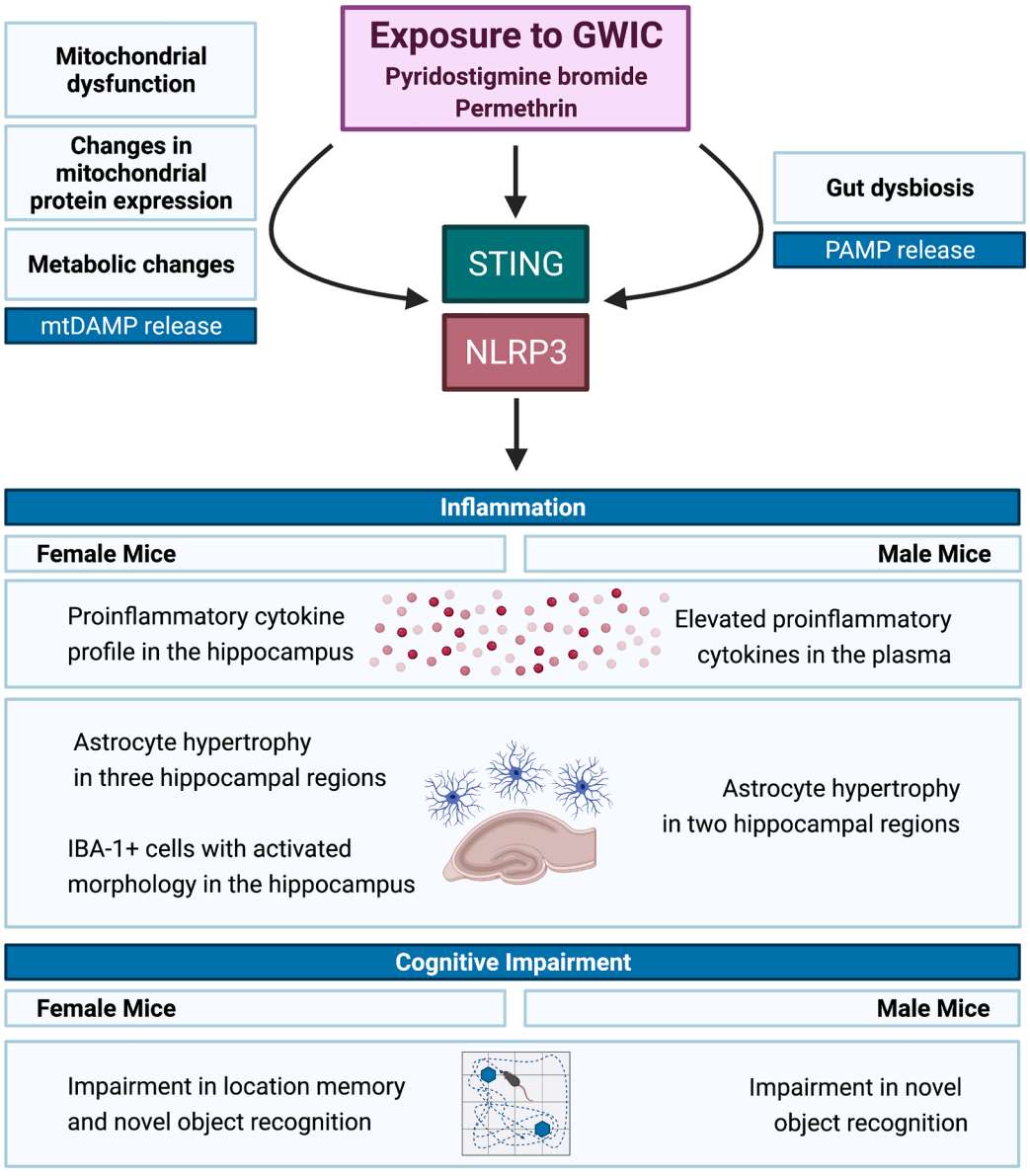

Fig. 5. Proposed model of the contribution of STING and NLRP3 to GWIC-related inflammation and cognitive impairment. Based on our data and other published studies, we developed the following model: GWIC exposure engages STING and NLRP3, resulting in inflammation and cognitive impairment. In our model, we observe sex differences in GWIC-dependent inflammation, with a proinflammatory cytokine profile and increased activated IBA-1+ cells seen in the hippocampi of female mice, and elevated proinflammatory cytokines seen in the plasma of male mice. GWIC-induced astrocyte hypertrophy was observed in both female and male mice, though it was more pronounced in females. In addition, we observed sex differences in GWIC-dependent cognitive impairment, with female mice showing impairment in both location memory and novel object recognition, while males show impairment in novel object recognition only. $STING^{gt/gt}$ and $NLRP3^{-/-}$ mice show attenuated inflammation and cognitive impairment, indicating that both signaling molecules are implicated in the inflammation and cognitive impairment observed downstream to GWIC exposure. We propose that GWIC engages STING and NLRP3 signaling through two mechanisms. First, GWIC exposure has been linked with gut dysbiosis (Seth et al., 2019; Alhasson et al., 2017; Bose et al., 2020), which results in the release of pathogen-associated molecular patterns (PAMPs) that can initiate STING and NLRP3 signaling pathways. In addition, GWIC exposure causes mitochondrial dysfunction (Shetty et al., 2017; Zakirova et al., 2017; Koslik et al., 2014; Golomb, 2014; Chen et al., 2017; Abdullah et al., 2016; Emmerich et al., 2017), supported by our results demonstrating GWIC-dependent changes in mitochondrial protein expression and metabolism. This could result in the release of mtDAMPs that can likewise engage STING and NLRP3, driving GWIC-dependent inflammation and cognitive impairment. Figure made with biorender.com.

dysfunction, which has been documented in veterans (Koslik et al., 2014; Golomb, 2014; Chen et al., 2017) and in animal models (Shetty et al., 2017; Zakirova et al., 2017; Abdullah et al., 2016; Emmerich et al., 2017), and confirmed by our *in vitro* studies (Supplementary Fig. 3), alters metabolism and promotes the exposure of mtDAMPS that trigger STING and/or NLRP3 to promote inflammatory processes in GWI. However, the endogenous ligand(s) that engage these signaling pathways downstream of GWIC-exposure remains unknown and will require further study to uncover. An additional possibility is that the gut dysbiosis and gut injury documented in GWI (Seth et al., 2019; Alhasson et al., 2017; Bose et al., 2020) generate pathogen-associated molecular patterns (PAMPs) that trigger STING and NLRP3, and that this process may supersede or synergize with mtDAMP production as a driver of inflammation during GWI.

An intriguing future direction is to evaluate whether pharmacological inhibitors of STING and NLRP3 can be utilized to treat aspects of GWI pathology. In addition, emerging links between mitochondria and the innate immune system raise the possibility that therapeutic approaches to improve mitochondrial health may also serve to decrease inflammation, likely by reducing mtDAMP release/accumulation. Therefore, future studies are warranted to determine whether mitochondria-targeted therapies can lower cognitive impairments and neuroinflammation in veterans with GWI.

Declaration of Competing Interest

The authors declare that they have no known competing financial interests or personal relationships that could have appeared to influence the work reported in this paper.

Acknowledgements

We thank Sahithi Attaluri for assistance with immunohistochemical analysis; Dr. Alexandra Trott, Associate Director of the TAMU Rodent Preclinical Phenotyping Core, for assistance with behavioral tests; and Dr. Jerome Trzeciakowski for assistance with statistical analysis. This work was supported, in part, by a grant from NIEHS P30 ESES029067 and by awards W81XWH-17-1-0446 (to A.P.W.), W81XWH-16-1-0480 (to A.K.S.), and W81XWH-17-1-0447 (to A.K.S.) from the Office of the Assistant Secretary of Defense for Health Affairs through the Peer Reviewed Medical Research Programs, Gulf War Illness Research Program. R.D. is funded by NIH grants (R01 CA193522 and R01 NS073939) and an MD Anderson Cancer Support Grant (P30 CA016672). Opinions, interpretations, conclusions, and recommendations are those of the authors and are not necessarily endorsed by the Department of Defense, NIH, or the United States Government.

Appendix A. Supplementary data

Supplementary data to this article can be found online at https://doi.org/10.1016/j.bbi.2021.07.015.

References

Abdullah, L., Crynen, G., Reed, J., Bishop, A., Phillips, J., Ferguson, S., Mouzon, B., Mullan, Myles, Mathura, V., Mullan, Michael, Ait-Ghezala, G., Crawford, F., 2011. Proteomic CNS profile of delayed cognitive impairment in mice exposed to Gulf War agents. Neuromol. Med. 13, 275–288. https://doi.org/10.1007/s12017-011-8160-z.

Abdullah, L., Evans, J.E., Bishop, A., Reed, J.M., Crynen, G., Phillips, J., Pelot, R., Mullan, M.A., Ferro, A., Mullan, C.M., Mullan, M.J., Ait-Ghezala, G., Crawford, F.C., 2012. Lipidomic profiling of phosphocholine-containing brain lipids in mice with sensorimotor deficits and anxiety-like features after exposure to Gulf War agents. Neuromol. Med. 14, 349–361. https://doi.org/10.1007/s12017-012-8192-z.

Abdullah, L., Evans, J.E., Joshi, U., Crynen, G., Reed, J., Mouzon, B., Baumann, S., Montague, H., Zakirova, Z., Emmerich, T., Bachmeier, C., Klimas, N., Sullivan, K., Mullan, M., Ait-Ghezala, G., Crawford, F., 2016. Translational potential of long-term decreases in mitochondrial lipids in a mouse model of Gulf War Illness. Toxicology 372, 22–33. https://doi.org/10.1016/j.tox.2016.10.012.

Alhasson, F., Das, S., Seth, R., Dattaroy, D., Chandrashekaran, V., Ryan, C.N., Chan, L.S., Testerman, T., Burch, J., Hofseth, L.J., Horner, R., Nagarkatti, M., Nagarkatti, P., Lasley, S.M., Chatterjee, S., 2017. Altered gut microbiome in a mouse model of Gulf War Illness causes neuroinflammation and intestinal injury via leaky gut and TLR4 activation. PLoS ONE 12. https://doi.org/10.1371/journal.pone.0172914.

Apaijai, N., Moisescu, D.M., Palee, S., McSweeney, C.M., Saiyasit, N., Maneechote, C., Boonnag, C., Chattipakorn, N., Chattipakorn, S.C., 2019. Pretreatment With PCSK9 inhibitor protects the brain against cardiac ischemia/reperfusion injury through a reduction of neuronal inflammation and amyloid beta aggregation. J. Am. Heart Assoc. 8 https://doi.org/10.1161/JAHA.118.010838.

Barber, G.N., 2015. STING: infection, inflammation and cancer. Nat. Rev. Immunol. 15, 760–770. https://doi.org/10.1038/nri3921.

Benkhoucha, M., Santiago-Raber, M.-L., Schneiter, G., Chofflon, M., Funakoshi, H., Nakamura, T., Lalive, P.H., 2010. Hepatocyte growth factor inhibits CNS autoimmunity by inducing tolerogenic dendritic cells and CD25+Foxp3+ regulatory T cells. Proc. Natl. Acad. Sci. U. S. A. 107, 6424–6429. https://doi.org/10.1073/pnas.0912437107.

Bingham, B., Shen, R., Kotnis, S., Lo, C.F., Ozenberger, B.A., Ghosh, N., Kennedy, J.D., Jacobsen, J.S., Grenier, J.M., DiStefano, P.S., Chiang, L.W., Wood, A., 2006. Proapoptotic effects of NARC 1 (= PCSK9), the gene encoding a novel serine proteinase. Cytom. Part J. Int. Soc. Anal. Cytol. 69, 1123–1131. https://doi.org/10.1002/cyto.a.20346.

Bose, D., Mondal, A., Saha, P., Kimono, D., Sarkar, S., Seth, R.K., Janulewicz, P., Sullivan, K., Horner, R., Klimas, N., Nagarkatti, M., Nagarkatti, P., Chatterjee, S., 2020. TLR antagonism by sparstolonin B alters microbial signature and modulates gastrointestinal and neuronal inflammation in gulf war illness preclinical model. Brain Sci. 10 https://doi.org/10.3390/brainsci10080532.

Broderick, G., Ben-Hamo, R., Vashishtha, S., Efroni, S., Nathanson, L., Barnes, Z., Fletcher, M.A., Klimas, N., 2013. Altered immune pathway activity under exercise challenge in Gulf War Illness: an exploratory analysis. Brain. Behav. Immun. 28, 159–169. https://doi.org/10.1016/j.bbi.2012.11.007.

Broderick, G., Kreitz, A., Fuite, J., Fletcher, M.A., Vernon, S.D., Klimas, N., 2011. A pilot study of immune network remodeling under challenge in Gulf War Illness. Brain. Behav. Immun. 25, 302–313. https://doi.org/10.1016/j.bbi.2010.10.011.

Butterick, T.A., Trembley, J.H., Hocum Stone, L.L., Muller, C.J., Rudquist, R.R., Bach, R. R., 2019. Gulf War Illness-associated increases in blood levels of interleukin 6 and C-reactive protein: biomarker evidence of inflammation. BMC Res. Notes 12, 816. https://doi.org/10.1186/s13104-019-4855-2.

Cameron, H.A., Hazel, T.G., McKay, R.D., 1998. Regulation of neurogenesis by growth factors and neurotransmitters. J. Neurobiol. 36, 287–306.

Castro-Marrero, J., Cordero, M.D., Sáez-Francas, N., Jimenez-Gutierrez, C., Aguilar-Montilla, F.J., Aliste, L., Alegre-Martin, J., 2013. Could mitochondrial dysfunction be a differentiating marker between chronic fatigue syndrome and fibromyalgia? Antioxid. Redox Signal. 19, 1855–1860. https://doi.org/10.1089/ars.2013.5346.

Chen, H., Xue, L.-X., Cao, H.-L., Chen, S.-W., Guo, Y., Gao, W.-W., Ju, S.-M., Tian, H.-L., 2013. Endostatin/collagen XVIII is increased in cerebrospinal fluid after severe traumatic brain injury. BioMed Res. Int. 2013 https://doi.org/10.1155/2013/402375.

Chen, Q., Sun, L., Chen, Z.J., 2016. Regulation and function of the cGAS-STING pathway of cytosolic DNA sensing. Nat. Immunol. 17, 1142–1149. https://doi.org/10.1038/ni.3558.

Chen, Y., Meyer, J.N., Hill, H.Z., Lange, G., Condon, M.R., Klein, J.C., Ndirangu, D., Falvo, M.J., 2017. Role of mitochondrial DNA damage and dysfunction in veterans with Gulf War Illness. PLoS One 12. https://doi.org/10.1371/journal.pone.0184832.

Coughlin, S.S., Coughlin, S.S., Krengel, M., Sullivan, K., Pierce, P.F., Heboyan, V., Wilson, L.C.C., Internationals, O., 2017. A Review of Epidemiologic Studies of the Health of Gulf War Women Veterans. J. Environ. Health Sci. 3.

Craddock, T.J.A., Harvey, J.M., Nathanson, L., Barnes, Z.M., Klimas, N.G., Fletcher, M.A., Broderick, G., 2015. Using gene expression signatures to identify novel treatment strategies in gulf war illness. BMC Med. Genomics 8, 36. https://doi.org/10.1186/s12920-015-0111-3.

Di Napoli, M., Elkind, M.S.V., Godoy, D.A., Singh, P., Papa, F., Popa-Wagner, A., 2011. Role of C-reactive protein in cerebrovascular disease: a critical review. Expert Rev. Cardiovasc. Ther. 9, 1565–1584. https://doi.org/10.1586/erc.11.159.

Elliott, E.I., Sutterwala, F.S., 2015. Initiation and perpetuation of NLRP3 inflammasome activation and assembly. Immunol. Rev. 265, 35–52. https://doi.org/10.1111/imr.12286.

Emmerich, T., Zakirova, Z., Klimas, N., Sullivan, K., Shetty, A.K., Evans, J.E., Ait-Ghezala, G., Laco, G.S., Hattiangady, B., Shetty, G.A., Mullan, M., Crynen, G., Abdullah, L., Crawford, F., 2017. Phospholipid profiling of plasma from GW veterans and rodent models to identify potential biomarkers of Gulf War Illness. PLoS ONE 12. https://doi.org/10.1371/journal.pone.0176634.

Fernández-Arjona, M.D.M., Grondona, J.M., Granados-Durán, P., Fernández-Llebrez, P., López-Ávalos, M.D., 2017. Microglia morphological categorization in a rat model of neuroinflammation by hierarchical cluster and principal components analysis. Front. Cell. Neurosci. 11, 235. https://doi.org/10.3389/fncel.2017.00235.

Freemerman, A.J., Johnson, A.R., Sacks, G.N., Milner, J.J., Kirk, E.L., Troester, M.A., Macintyre, A.N., Goraksha-Hicks, P., Rathmell, J.C., Makowski, L., 2014. Metabolic Reprogramming of Macrophages: glucose transporter 1 (GLUT1)-mediated glucose metabolism drives a proinflammatory phenotype*. J. Biol. Chem. 289, 7884–7896. https://doi.org/10.1074/jbc.M113.522037.

Gao, D., Wu, J., Wu, Y.-T., Du, F., Aroh, C., Yan, N., Sun, L., Chen, Z.J., 2013. Cyclic GMP-AMP synthase is an innate immune sensor of HIV and other retroviruses. Science 341, 903–906. https://doi.org/10.1126/science.1240933.

Goasdoue, K., Chand, K.K., Miller, S.M., Lee, K.M., Colditz, P.B., Wixey, J.A., Bjorkman, S.T., 2019. Seizures are associated with blood-brain barrier disruption in a piglet model of neonatal hypoxic-ischaemic encephalopathy. Dev. Neurosci. 1–16 https://doi.org/10.1159/000499365.

Golomb, B.A., 2008. Acetylcholinesterase inhibitors and Gulf War illnesses. Proc. Natl. Acad. Sci. U. S. A. 105, 4295–4300. https://doi.org/10.1073/pnas.0711986105.

Golomb, B.A., Allison, M., Koperski, S., Koslik, H.J., Devaraj, S., Ritchie, J.B., 2014. Coenzyme Q10 benefits symptoms in Gulf War veterans: results of a randomized double-blind study. Neural Comput. 26, 2594–2651. https://doi.org/10.1162/NECO_a_00659.

Grossberg, A.J., Vichaya, E.G., Gross, P.S., Ford, B.G., Scott, K.A., Estrada, D., Vermeer, D.W., Vermeer, P., Dantzer, R., 2020. Interleukin 6-independent metabolic reprogramming as a driver of cancer-related fatigue. Brain. Behav. Immun. 88, 230–241. https://doi.org/10.1016/j.bbi.2020.05.043.

Hattiangady, B., Mishra, V., Kodali, M., Shuai, B., Rao, X., Shetty, A.K., 2014. Object location and object recognition memory impairments, motivation deficits and depression in a model of Gulf War illness. Front. Behav. Neurosci. 8, 78. https://doi.org/10.3389/fnbeh.2014.00078.

Heboyan, V., Krengel, M.H., Sullivan, K., Iobst, S., Klimas, N., Wilson, C., Coughlin, S.S., 2019. Sex differences in gulf war illness: a reanalysis of data from the CDC air force study using CDC and modified kansas case definitions. J. Occup. Environ. Med. 61, 610–616. https://doi.org/10.1097/JOM.0000000000001620.

James, L.M., Engdahl, B.E., Johnson, R.A., Georgopoulos, A.P., 2019. Gulf War Illness and Inflammation: association of symptom severity with C-reactive protein. J. Neurol. Neuromed. 4.

Janulewicz, P.A., Seth, R.K., Carlson, J.M., Ajama, J., Quinn, E., Heeren, T., Klimas, N., Lasley, S.M., Horner, R.D., Sullivan, K., Chatterjee, S., 2019. The gut-microbiome in gulf war veterans: a preliminary report. Int. J. Environ. Res. Public. Health 16. https://doi.org/10.3390/ijerph16193751.

Jeon, H., Lee, S., Lee, W.-H., Suk, K., 2010. Analysis of glial secretome: the long pentraxin PTX3 modulates phagocytic activity of microglia. J. Neuroimmunol. 229, 63–72. https://doi.org/10.1016/j.jneuroim.2010.07.001.

Johnson, G.J., Slater, B.C.S., Leis, L.A., Rector, T.S., Bach, R.R., 2016. blood biomarkers of chronic inflammation in Gulf War illness. PloS One 11. https://doi.org/10.1371/journal.pone.0157855.

Joshi, U., Evans, J.E., Joseph, R., Emmerich, T., Saltiel, N., Lungmus, C., Oberlin, S., Langlois, H., Ojo, J., Mouzon, B., Paris, D., Mullan, M., Jin, C., Klimas, N., Sullivan, K., Crawford, F., Abdullah, L., 2018. Oleoylethanolamide treatment reduces neurobehavioral deficits and brain pathology in a mouse model of Gulf War Illness. Sci. Rep. 8, 12921. https://doi.org/10.1038/s41598-018-31242-7.

Joshi, U., Evans, J.E., Pearson, A., Saltiel, N., Cseresznye, A., Darcey, T., Ojo, J., Keegan, A.P., Oberlin, S., Mouzon, B., Paris, D., Klimas, N., Sullivan, K., Mullan, M.,

Crawford, F., Abdullah, L., 2020. Targeting sirtuin activity with nicotinamide riboside reduces neuroinflammation in a GWI mouse model. Neurotoxicology 79, 84–94. https://doi.org/10.1016/j.neuro.2020.04.006.

Juma, W.M., Lira, A., Marzuk, A., Marzuk, Z., Hakim, A.M., Thompson, C.S., 2011. C-reactive protein expression in a rodent model of chronic cerebral hypoperfusion. Brain Res. 1414, 85–93. https://doi.org/10.1016/j.brainres.2011.07.047.

Kato, T., Funakoshi, H., Kadoyama, K., Noma, S., Kanai, M., Ohya-Shimada, W., Mizuno, S., Doe, N., Taniguchi, T., Nakamura, T., 2012. Hepatocyte growth factor overexpression in the nervous system enhances learning and memory performance in mice. J. Neurosci. Res. 90, 1743–1755. https://doi.org/10.1002/jnr.23065.

Kelly, B., O'Neill, L.A., 2015. Metabolic reprogramming in macrophages and dendritic cells in innate immunity. Cell Res. 25, 771–784. https://doi.org/10.1038/cr.2015.68.

Klein, S.L., Flanagan, K.L., 2016. Sex differences in immune responses. Nat. Rev. Immunol. 16, 626–638. https://doi.org/10.1038/nri.2016.90.

Klemm, A.H., 2020. Semi-automated analysis of dot blots using ImageJ/Fiji. F1000Research 9, 1385. https://doi.org/10.12688/f1000research.27179.1.

Kodali, M., Hattiangady, B., Shetty, G.A., Bates, A., Shuai, B., Shetty, A.K., 2018. Curcumin treatment leads to better cognitive and mood function in a model of Gulf War Illness with enhanced neurogenesis, and alleviation of inflammation and mitochondrial dysfunction in the hippocampus. Brain. Behav. Immun. 69, 499–514. https://doi.org/10.1016/j.bbi.2018.01.009.

Koslik, H.J., Hamilton, G., Golomb, B.A., 2014. Mitochondrial dysfunction in Gulf War illness revealed by 31Phosphorus Magnetic Resonance Spectroscopy: a case-control study. PLoS One 9. https://doi.org/10.1371/journal.pone.0092887.

Kovarova, M., Hesker, P.R., Jania, L., Nguyen, M., Snouwaert, J.N., Xiang, Z., Lommatzsch, S.E., Huang, M.T., Ting, J.P.-Y., Koller, B.H., 2012. NLRP1-dependent pyroptosis leads to acute lung injury and morbidity in mice. J. Immunol. Baltim. Md 1950 (189), 2006–2016. https://doi.org/10.4049/jimmunol.1201065.

Li, N., Zhou, H., Wu, H., Wu, Q., Duan, M., Deng, W., Tang, Q., 2019. STING-IRF3 contributes to lipopolysaccharide-induced cardiac dysfunction, inflammation, apoptosis and pyroptosis by activating NLRP3. Redox Biol. 24 https://doi.org/10.1016/j.redox.2019.101215.

Madhu, L.N., Attaluri, S., Kodali, M., Shuai, B., Upadhya, R., Gitai, D., Shetty, A.K., 2019. Neuroinflammation in Gulf War Illness is linked with HMGB1 and complement activation, which can be discerned from brain-derived extracellular vesicles in the blood. Brain. Behav. Immun. 81, 430–443. https://doi.org/10.1016/j.bbi.2019.06.040.

Malik, A.R., Lips, J., Gorniak-Walas, M., Broekaart, D.W.M., Asaro, A., Kuffner, M.T.C., Hoffmann, C.J., Kikhia, M., Dopatka, M., Boehm-Sturm, P., Mueller, S., Dirnagl, U., Aronica, E., Harms, C., Willnow, T.E., 2020. SorCS2 facilitates release of endostatin from astrocytes and controls post-stroke angiogenesis. Glia 68, 1304–1316. https://doi.org/10.1002/glia.23778.

Malla, K.K., Malla, T., Rao, K.S., Basnet, S., Shah, R., 2013. Is Cerebrospinal fluid C-reactive protein a better tool than blood C-reactive protein in laboratory diagnosis of meningitis in children? Sultan Qaboos Univ. Med. J. 13, 93–99. https://doi.org/10.12816/0003201.

Man, S.M., Kanneganti, T.-D., 2016. Converging roles of caspases in inflammasome activation, cell death and innate immunity. Nat. Rev. Immunol. 16, 7–21. https://doi.org/10.1038/nri.2015.7.

Mauvais-Jarvis, F., Merz, N.B., Barnes, P.J., Brinton, R.D., Carrero, J.-J., DeMeo, D.L., Vries, G.J.D., Epperson, C.N., Govindan, R., Klein, S.L., Lonardo, A., Maki, P.M., McCullough, L.D., Regitz-Zagrosek, V., Regensteiner, J.G., Rubin, J.B., Sandberg, K., Suzuki, A., 2020. Sex and gender: modifiers of health, disease, and medicine. The Lancet 396, 565–582. https://doi.org/10.1016/S0140-6736(20)31561-0.

Nakahira, K., Hisata, S., Choi, A.M.K., 2015. The roles of mitochondrial damage-associated molecular patterns in diseases. Antioxid. Redox Signal. 23, 1329–1350. https://doi.org/10.1089/ars.2015.6407.

Ni, P., Dong, H., Wang, Y., Zhou, Q., Xu, M., Qian, Y., Sun, J., 2018. IL-17A contributes to perioperative neurocognitive disorders through blood-brain barrier disruption in aged mice. J. Neuroinflammation 15, 332. https://doi.org/10.1186/s12974-018-1374-3.

Niimura, M., Takagi, N., Takagi, K., Mizutani, R., Tanonaka, K., Funakoshi, H., Matsumoto, K., Nakamura, T., Takeo, S., 2006. The protective effect of hepatocyte growth factor against cell death in the hippocampus after transient forebrain ischemia is related to the improvement of apurinic/apyrimidinic endonuclease/redox factor-1 level and inhibition of NADPH oxidase activity. Neurosci. Lett. 407, 136–140. https://doi.org/10.1016/j.neulet.2006.08.060.

Ojo, J.O., Abdullah, L., Evans, J., Reed, J.M., Montague, H., Mullan, M.J., Crawford, F.C., 2014. Exposure to an organophosphate pesticide, individually or in combination with other Gulf War agents, impairs synaptic integrity and neuronal differentiation, and is accompanied by subtle microvascular injury in a mouse model of Gulf War agent exposure. Neuropathol. Off. J. Jpn. Soc. Neuropathol. 34, 109–127. https://doi.org/10.1111/neup.12061.

Parkitny, L., Middleton, S., Baker, K., Younger, J., 2015. Evidence for abnormal cytokine expression in Gulf War Illness: A preliminary analysis of daily immune monitoring data. BMC Immunol. 16, 57. https://doi.org/10.1186/s12865-015-0122-z.

Patten, E., Parker, K., 2011. Women in the U.S. Military: Growing Share, Distinctive Profile. Pew Res. Center's Soc. Demogr. Trends Proj. URL https://www.pewresearch.org/social-trends/2011/12/22/women-in-the-u-s-military-growing-share-distinctive-profile/ (accessed 7.13.21).

Pierce, P.F., 2005. Federal nursing service awardmonitoring the health of Persian Gulf War veteran women. Mil. Med. 170, 349–354. https://doi.org/10.7205/MILMED.170.5.349.

Planas, A.M., Solé, S., Justicia, C., 2001. Expression and activation of matrix metalloproteinase-2 and -9 in rat brain after transient focal cerebral ischemia. Neurobiol. Dis. 8, 834–846. https://doi.org/10.1006/nbdi.2001.0435.

Roers, A., Hiller, B., Hornung, V., 2016. Recognition of endogenous nucleic acids by the innate immune system. Immunity 44, 739–754. https://doi.org/10.1016/j.immuni.2016.04.002.

Ryu, W.-S., Kim, C.K., Kim, B.J., Kim, C., Lee, S.-H., Yoon, B.-W., 2012. Pentraxin 3: a novel and independent prognostic marker in ischemic stroke. Atherosclerosis 220, 581–586. https://doi.org/10.1016/j.atherosclerosis.2011.11.036.

Sauer, J.-D., Sotelo-Troha, K., von Moltke, J., Monroe, K.M., Rae, C.S., Brubaker, S.W., Hyodo, M., Hayakawa, Y., Woodward, J.J., Portnoy, D.A., Vance, R.E., 2011. The N-ethyl-N-nitrosourea-induced Goldenticket mouse mutant reveals an essential function of Sting in the in vivo interferon response to Listeria monocytogenes and cyclic dinucleotides. Infect. Immun. 79, 688–694. https://doi.org/10.1128/IAI.00999-10.

Seth, R.K., Maqsood, R., Mondal, A., Bose, D., Kimono, D., Holland, L.A., Janulewicz Lloyd, P., Klimas, N., Horner, R.D., Sullivan, K., Lim, E.S., Chatterjee, S., 2019. Gut DNA virome diversity and its association with host bacteria regulate inflammatory phenotype and neuronal immunotoxicity in experimental gulf war illness. Viruses 11. https://doi.org/10.3390/v11100968.

Shetty, A.K., Attaluri, S., Kodali, M., Shuai, B., Shetty, G.A., Upadhya, D., Hattiangady, B., Madhu, L.N., Upadhya, R., Bates, A., Rao, X., 2020. Monosodium luminol reinstates redox homeostasis, improves cognition, mood and neurogenesis, and alleviates neuro- and systemic inflammation in a model of Gulf War Illness. Redox Biol. 28 https://doi.org/10.1016/j.redox.2019.101389.

Shetty, G.A., Hattiangady, B., Upadhya, D., Bates, A., Attaluri, S., Shuai, B., Kodali, M., Shetty, A.K., 2017. Chronic oxidative stress, mitochondrial dysfunction, Nrf2 activation and inflammation in the hippocampus accompany heightened systemic inflammation and oxidative stress in an animal model of gulf war illness. Front. Mol. Neurosci. 10 https://doi.org/10.3389/fnmol.2017.00182.

Shindo, A., Maki, T., Mandeville, E.T., Liang, A.C., Egawa, N., Itoh, K., Itoh, N., Borlongan, M., Holder, J.C., Chuang, T.T., McNeish, J.D., Tomimoto, H., Lok, J., Lo, E.H., Arai, K., 2016. Astrocyte-derived pentraxin 3 supports blood-brain barrier integrity under acute phase of stroke. Stroke 47, 1094–1100. https://doi.org/10.1161/STROKEAHA.115.012133.

Turbic, A., Leong, S.Y., Turnley, A.M., 2011. Chemokines and inflammatory mediators interact to regulate adult murine neural precursor cell proliferation, survival and differentiation. PLoS One 6. https://doi.org/10.1371/journal.pone.0025406.

West, A.P., 2017. Mitochondrial dysfunction as a trigger of innate immune responses and inflammation. Toxicology 391, 54–63. https://doi.org/10.1016/j.tox.2017.07.016.

West, A.P., Shadel, G.S., Ghosh, S., 2011. Mitochondria in innate immune responses. Nat. Rev. Immunol. 11, 389–402. https://doi.org/10.1038/nri2975.

White, R.F., Steele, L., O'Callaghan, J.P., Sullivan, K., Binns, J.H., Golomb, B.A., Bloom, F.E., Bunker, J.A., Crawford, F., Graves, J.C., Hardie, A., Klimas, N., Knox, M., Meggs, W.J., Melling, J., Philbert, M.A., Grashow, R., 2016. Recent research on Gulf War illness and other health problems in veterans of the 1991 Gulf War: Effects of toxicant exposures during deployment. Cortex. J. Devoted Study Nerv. Syst. Behav. 74, 449–475. https://doi.org/10.1016/j.cortex.2015.08.022.

Wight, R.D., Tull, C.A., Deel, M.W., Stroope, B.L., Eubanks, A.G., Chavis, J.A., Drew, P.D., Hensley, L.L., 2012. Resveratrol effects on astrocyte function: relevance to neurodegenerative diseases. Biochem. Biophys. Res. Commun. 426, 112–115. https://doi.org/10.1016/j.bbrc.2012.08.045.

Wong, R.W.C., Guillaud, L., 2004. The role of epidermal growth factor and its receptors in mammalian CNS. Cytokine Growth Factor Rev. 15, 147–156. https://doi.org/10.1016/j.cytogfr.2004.01.004.

Yamada, M., Ikeuchi, T., Hatanaka, H., 1997. The neurotrophic action and signalling of epidermal growth factor. Prog. Neurobiol. 51, 19–37. https://doi.org/10.1016/s0301-0082(96)00046-9.

Yasojima, K., Schwab, C., McGeer, E.G., McGeer, P.L., 2000. Human neurons generate C-reactive protein and amyloid P: upregulation in Alzheimer's disease. Brain Res. 887, 80–89. https://doi.org/10.1016/s0006-8993(00)02970-x.

Yin, Y., Guo, R., Shao, Y., Ge, M., Miao, C., Cao, L., Yang, Y., Hu, L., 2019. Pretreatment with resveratrol ameliorate trigeminal neuralgia by suppressing matrix metalloproteinase-9/2 in trigeminal ganglion. Int. Immunopharmacol. 72, 339–347. https://doi.org/10.1016/j.intimp.2019.04.014.

Zakirova, Z., Crynen, G., Hassan, S., Abdullah, L., Horne, L., Mathura, V., Crawford, F., Ait-Ghezala, G., 2015. A chronic longitudinal characterization of neurobehavioral and neuropathological cognitive impairment in a mouse model of gulf war agent exposure. Front. Integr. Neurosci. 9, 71. https://doi.org/10.3389/fnint.2015.00071.

Zakirova, Z., Reed, J., Crynen, G., Horne, L., Hassan, S., Mathura, V., Mullan, M., Crawford, F., Ait-Ghezala, G., 2017. Complementary proteomic approaches reveal mitochondrial dysfunction, immune and inflammatory dysregulation in a mouse model of Gulf War Illness. Proteomics Clin. Appl. 11 https://doi.org/10.1002/prca.201600190.

Zakirova, Z., Tweed, M., Crynen, G., Reed, J., Abdullah, L., Nissanka, N., Mullan, M., Mullan, M.J., Mathura, V., Crawford, F., Ait-Ghezala, G., 2015. Gulf War agent exposure causes impairment of long-term memory formation and neuropathological changes in a mouse model of Gulf War Illness. PloS One 10. https://doi.org/10.1371/journal.pone.0119579.

Zhang, B., Zhang, H.-X., Shi, S.-T., Bai, Y.-L., Zhe, X., Zhang, S.-J., Li, Y.-J., 2019. Interleukin-11 treatment protected against cerebral ischemia/reperfusion injury. Biomed. Pharmacother. Biomedecine Pharmacother. 115 https://doi.org/10.1016/j.biopha.2019.108816.

Zhang, C., Qian, S., Zhang, R., Guo, D., Wang, A., Peng, Y., Peng, H., Li, Q., Ju, Z., Geng, D., Chen, J., Zhang, Y., He, J., Zhong, C., Xu, T., 2020. Endostatin as a novel

prognostic biomarker in acute ischemic stroke. Atherosclerosis 293, 42–48. https://doi.org/10.1016/j.atherosclerosis.2019.11.032.

Zhang, H.-Y., Wang, Y., He, Y., Wang, T., Huang, X.-H., Zhao, C.-M., Zhang, L., Li, S.-W., Wang, C., Qu, Y.-N., Jiang, X.-X., 2020. A1 astrocytes contribute to murine depression-like behavior and cognitive dysfunction, which can be alleviated by IL-10 or fluorocitrate treatment. J. Neuroinflammation 17, 200. https://doi.org/10.1186/s12974-020-01871-9.

Zhang, Q., Zhou, X.D., Denny, T., Ottenweller, J.E., Lange, G., LaManca, J.J., Lavietes, M. H., Pollet, C., Gause, W.C., Natelson, B.H., 1999. Changes in immune parameters seen in Gulf War veterans but not in civilians with chronic fatigue syndrome. Clin. Diagn. Lab. Immunol. 6, 6–13.

Zundel, C.G., Krengel, M.H., Heeren, T., Yee, M.K., Grasso, C.M., Janulewicz Lloyd, P.A., Coughlin, S.S., Sullivan, K., 2019. Rates of chronic medical conditions in 1991 Gulf War Veterans compared to the general population. Int. J. Environ. Res. Public. Health 16. https://doi.org/10.3390/ijerph16060949.

Supplementary Figure 1

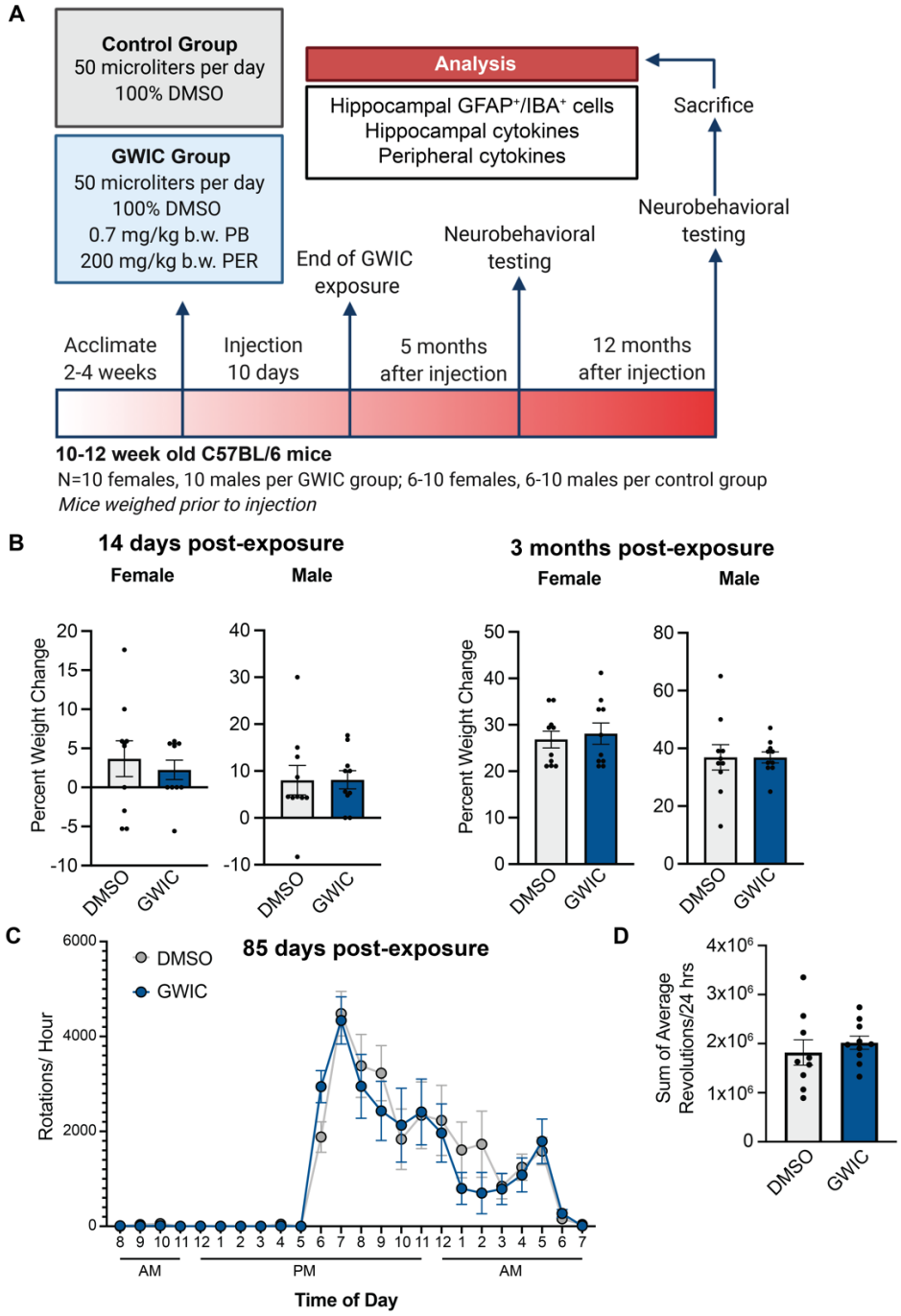

Supplementary Figure 1. The experimental GWI model used in this study does not result in changes in weight gain or voluntary wheel running activity. (A) This diagram summarizes the design for studies using the GWIC-exposure murine model of GWI. C57BL/6 mice (10 female and 10 male mice for GWIC groups, 6-10 female and 6-10 male mice for control groups) were allowed to acclimate for 2-4 weeks to the animal facility. After weighing, these mice, which were 12 weeks of age, were then injected daily with 50 microliters of 100% DMSO (control group) or 50 microliters of 100% DMSO containing 0.7 milligrams per kilogram body weight pyridostigmine bromide (PB) and 200 milligrams per kilogram body weight permethrin (Per) (GWIC group). Daily injections occurred for 10 consecutive days, then ceased. Five and twelve months after injection, all mice were subjected to neurobehavioral testing. Following behavioral testing at twelve months, mice were then euthanized to allow for analysis of GFAP+ and IBA+ cells in the hippocampus and expression of hippocampal and plasma cytokines. (B) Percent weight change in C57BL/6 wild-type female and male DMSO- and GWIC-exposed mice at 14 days and 3 months post exposure. Data represented as mean ± SEM of biological replicates, N=10. (C) Hourly wheel running activity in DMSO- and GWIC-exposed mice 85 days post GWIC-exposure. Data represented as mean ± SEM of biological replicates, N=9-10. Statistics calculated using 2-way ANOVA (factor = treatment, $F(1,408) = 0.6084$, $p = 0.4359$). (D) Sum of average daily wheel revolutions for DMSO- and GWIC-exposed mice 85 days post GWIC-exposure. Data represented as mean ± SEM of biological replicates, N=9-10. Statistics calculated using two-tailed t-test ($t = 0.7665$, $df = 8$, $p = 0.4654$).

Supplementary Figure 2

A

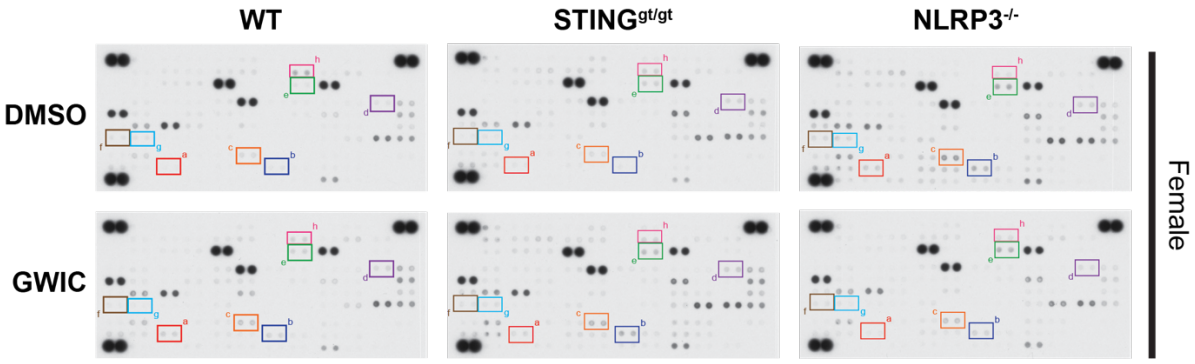

B

Cytokine	Female FC (GWIC/DMSO) WT	Female FC (GWIC/DMSO) STINGgt/gt	Female FC (GWIC/DMSO) NLRP3-/-	Male FC (GWIC/DMSO) WT	Male FC (GWIC/DMSO) STINGgt/gt	Male FC (GWIC/DMSO) NLRP3-/-
Pentraxin 3[a]	5.30	3.12	0.49	0.97	2.77	0.46
PCSK9[b]	2.83	11.35	0.71	1.05	1.30	0.73
MMP-2[c]	2.39	4.21	0.62	0.87	1.24	0.74
Endostatin[d]	2.03	2.02	1.61	0.89	1.70	0.61
CRP[e]	1.96	1.81	1.23	1.36	1.35	0.98
IL-10[f]	0.47	2.71	2.09	0.90	1.62	2.45
IL-11[g]	0.49	1.90	1.25	1.38	1.82	1.02
CCL21[h]	0.37	0.92	NC	0.67	1.71	0.58

Factors most changed in female mice

C

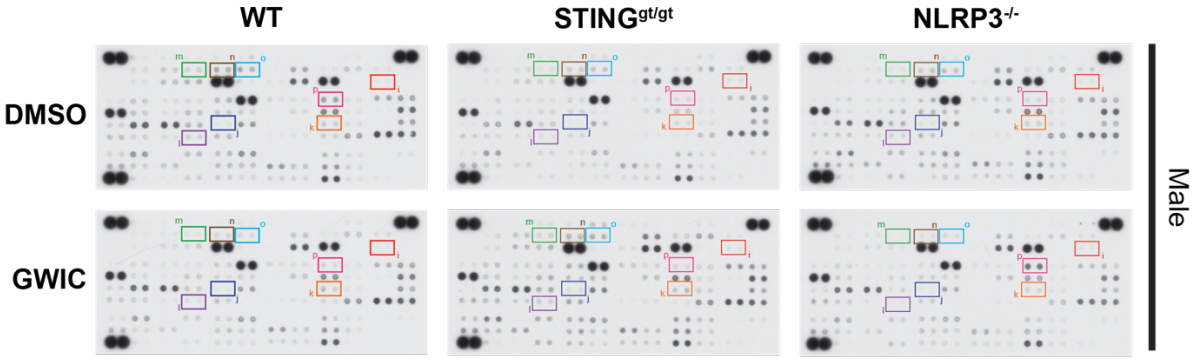

D

Cytokine	Female FC (GWIC/DMSO) WT	Female FC (GWIC/DMSO) STINGgt/gt	Female FC (GWIC/DMSO) NLRP3-/-	Male FC (GWIC/DMSO) WT	Male FC (GWIC/DMSO) STINGgt/gt	Male FC (GWIC/DMSO) NLRP3-/-
HGF[i]	1.45	2.22	NC	2.52	1.61	1.06
IL-1β[j]	NC	NC	NC	1.52	2.90	NC
IL-4[k]	NC	1.76	1.54	1.71	2.47	1.00
IL-13[l]	NC	NC	NC	0.54	2.29	0.36
CCL12[m]	NC	1.28	0.35	0.40	1.67	0.73
CCL17[n]	1.07	0.83	NC	0.34	1.45	0.30
CCL19[o]	0.91	0.85	NC	0.35	1.33	0.34
EGF[p]	NC	1.07	NC	0.27	1.04	12.24

Factors most changed in male mice

Supplementary Figure 2. GWIC exposure induces changes in hippocampal cytokine expression. Hippocampal protein lysates were generated from WT, STING$^{gt/gt}$, and NLRP3$^{-/-}$ DMSO- and GWIC-exposed female (A, B) and male (C, D) mice at 12 months post-exposure. Lysates from 4 mice for each group were pooled and analyzed on Mouse XL Cytokine Arrays. Each cytokine in the array is represented by a duplicate pair of spots. The integrated pixel density was measured for each spot and averaged for each cytokine. Fold change was calculated by dividing the mean pixel intensity for each cytokine in the GWIC-exposed group by the pixel intensity in the DMSO control group. "NC" indicates that fold change could not be calculated because one or both cytokines were below the limit of detection (see Section 2.4.2 of Materials and Methods for more details).

Supplementary Figure 3

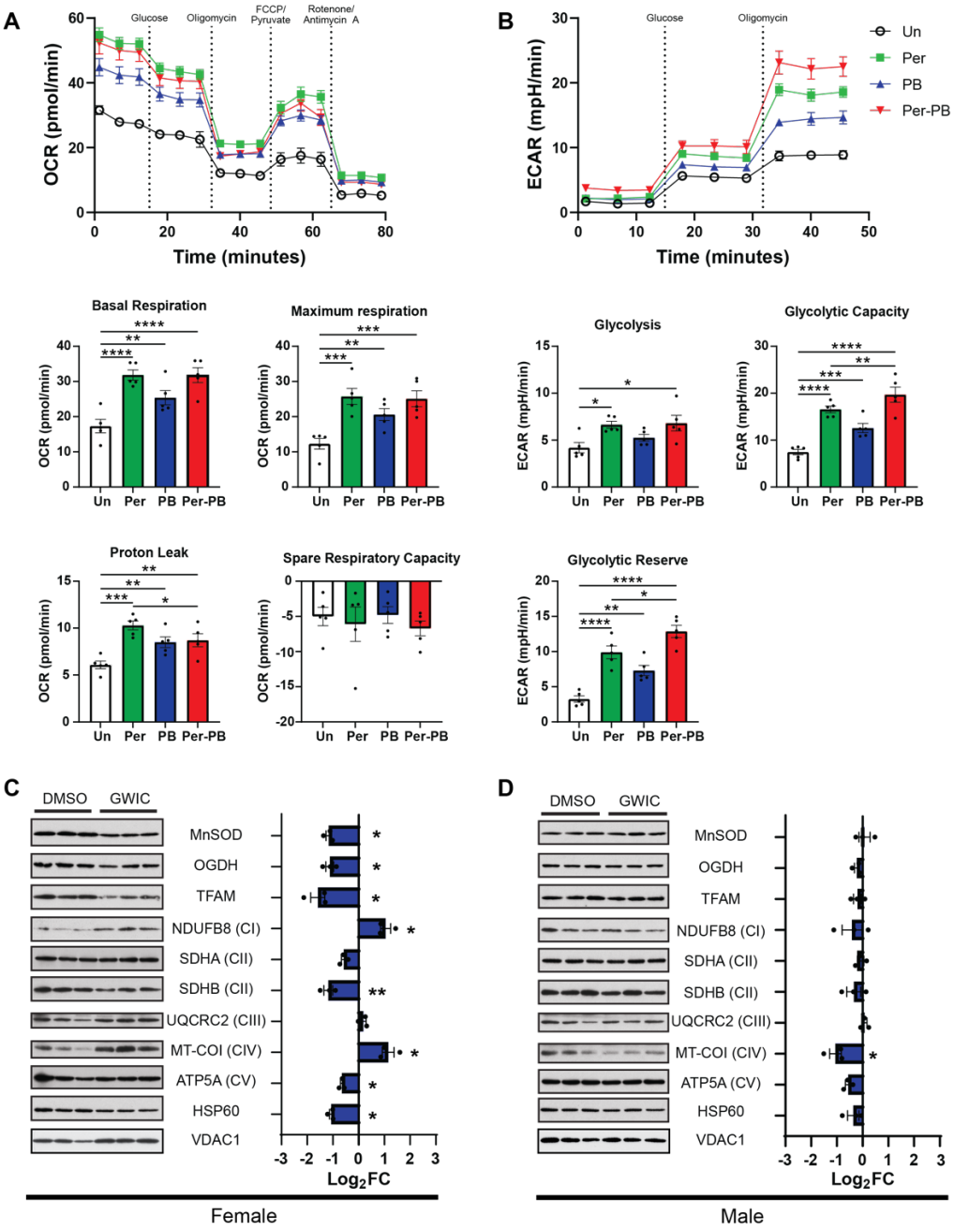

Supplementary Figure 3. GWIC exposure alters respiration and glycolysis in LPS-treated BMDMs and induces rewiring of mitochondrial protein expression in the hippocampus of female mice. Oxygen consumption rate (OCR, A) and extracellular acidification rate (ECAR, B) in LPS-stimulated BMDMs treated with GWICs. BMDMs were treated for 3 days with GWICs as indicated. Cells were treated with 200 ng/mL LPS (LPS) for 6 hours, then OCR and ECAR were measured on a Seahorse XF96 Analyzer using a modified protocol as described in Section 2.9 of Materials and Methods. Significance values for *post hoc* pairwise comparisons after one-way ANOVA were calculated using the two-stage step-up method to yield q values that have been corrected for the false discovery rate. * $q < 0.05$; ** $q < 0.01$; *** $q < 0.001$; **** $q < 0.0001$. At 12 months post-exposure, tissue extracts were generated from microdissected hippocampi from DMSO- and GWIC-exposed female mice (C) and male mice (D) and immunoblotted for the listed proteins as described in Section 2.6 of Materials and Methods. Labels in parentheses next to listed proteins designate proteins as part of complex I (CI), complex II (CII), complex III (CIII), complex IV (CIV) or complex V (CV) of the electron transport chain. Densitometry for each protein was performed in ImageJ and normalized to the VDAC expression level. Bars represent the $\log_2$ fold change (FC) of biological replicates +/- SEM (N=3). Indicated p-values were calculated using a two-tailed, unpaired, Student's t-test. *$p < 0.05$; **$p < 0.01$.

Supplementary Figure 4

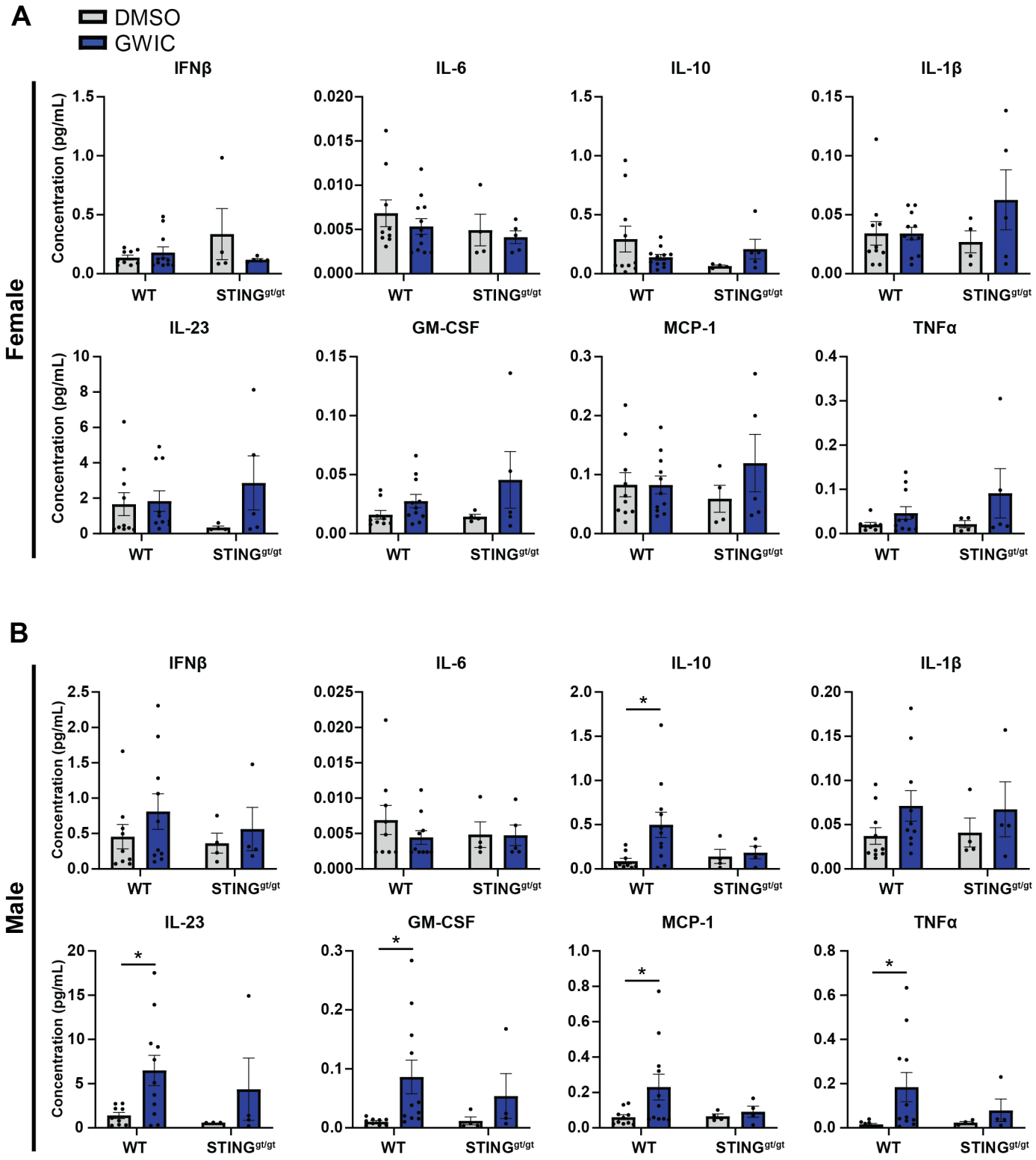

Supplementary Figure 4. Loss of STING partially rescues elevated plasma inflammatory cytokines in GWIC-exposed male mice. Peripheral cytokines measured in plasma collected from STING$^{gt/gt}$ DMSO- and GWIC-exposed female (A) and male (B) mice at 12 months post-exposure. Bars represent the mean concentration of biological replicates +/- SEM (N=4 for STING$^{gt/gt}$ DMSO females (A), N=5 for STING$^{gt/gt}$ GWIC females (A), N=4 for STING$^{gt/gt}$ DMSO males (B), N=4 for STING$^{gt/gt}$ GWIC males (B)). Cytokine concentrations from WT mice in Figure 3E are included as a reference for comparison. Indicated p-values were calculated using a two-tailed, unpaired, Student's t-test. *$p < 0.05$;.

Supplementary Figure 5

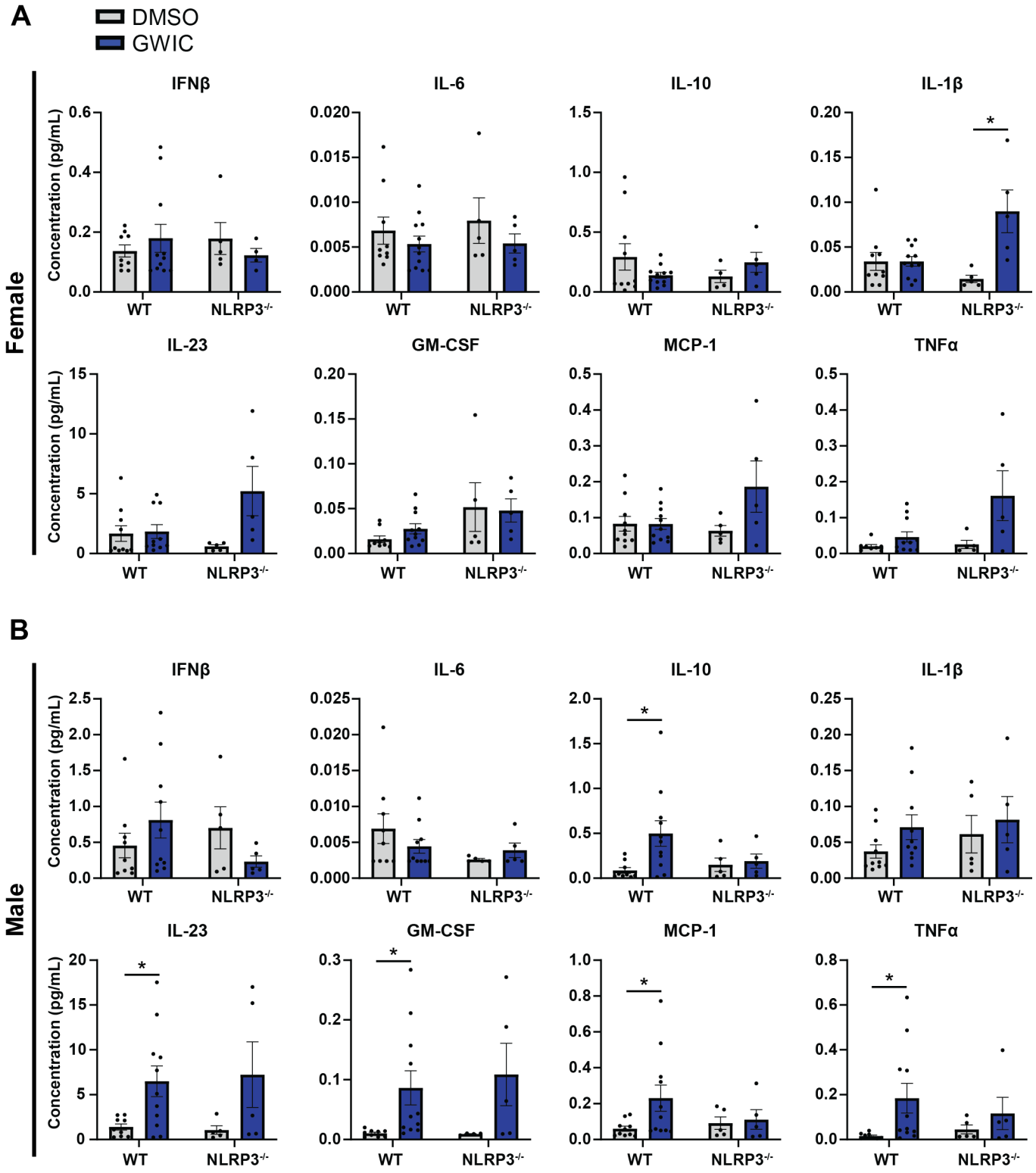

Supplementary Figure 5. Loss of NLRP3 partially rescues elevated plasma inflammatory cytokines in GWIC-exposed male mice. Peripheral cytokines measured in plasma collected from NLRP3$^{-/-}$ DMSO- and GWIC-exposed female (A) and male (B) mice at 12 months post-exposure. Bars represent the mean concentration of biological replicates +/- SEM (N=5 for NLRP3$^{-/-}$ DMSO females (A), N=5 for NLRP3$^{-/-}$ GWIC females (A), N=5 for NLRP3$^{-/-}$ DMSO males (B), N=5 for NLRP3$^{-/-}$ GWIC males (B)). Cytokine concentrations from WT mice in Figure 3E are included as a reference for comparison. Indicated p-values were calculated using a two-tailed, unpaired, Student's t-test. *$p < 0.05$;.

Supplementary Figure 6

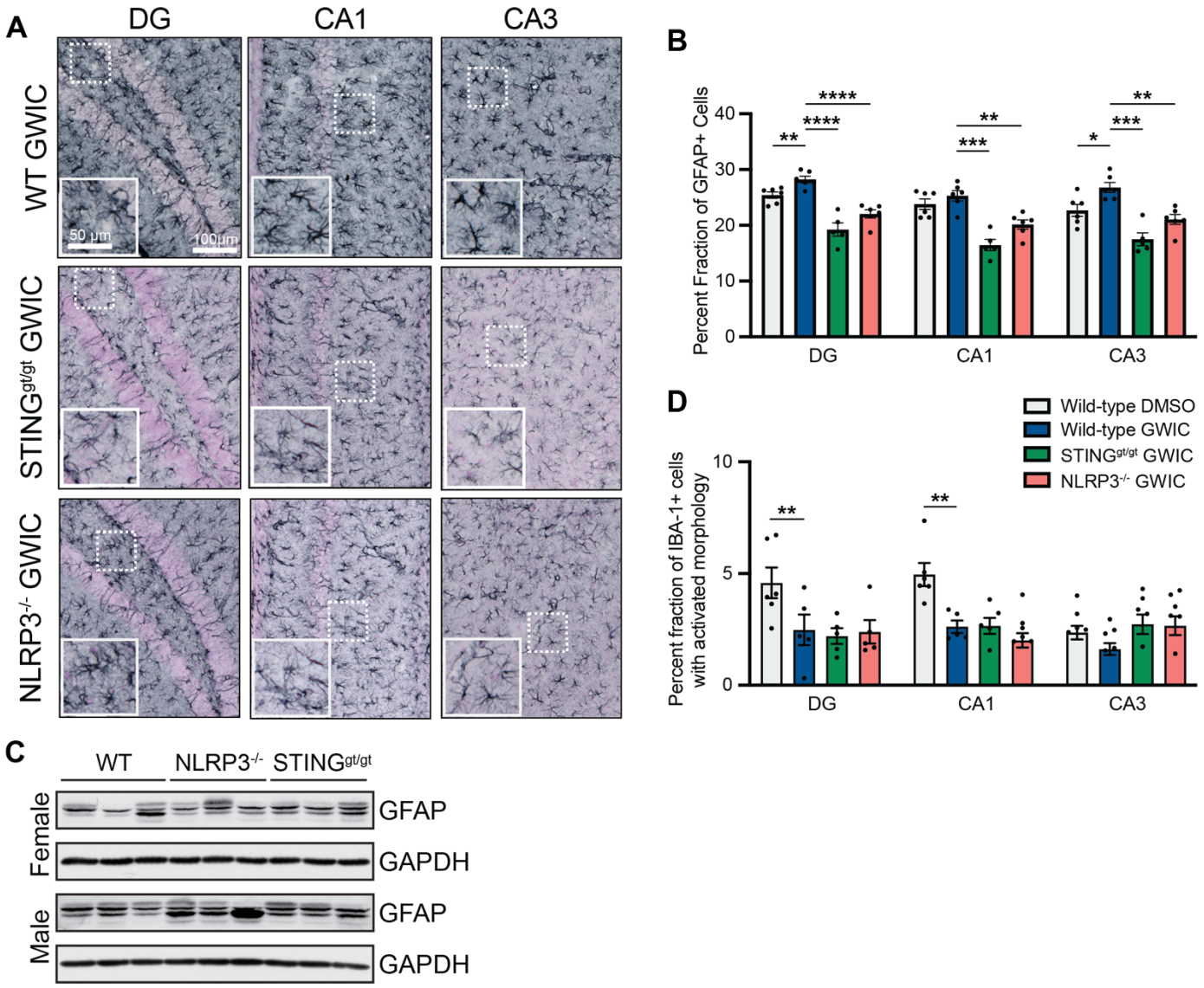

Supplementary Figure 6. Percent fraction of GFAP+ cells, GFAP expression, and IBA-1+ cells in the hippocampi of STING$^{gt/gt}$ and NLRP3$^{-/-}$ GWIC-exposed male mice. (A) Images show representative distribution and morphology of GFAP+ astrocytes in these three regions in WT, STING$^{gt/gt}$, and NLRP3$^{-/-}$ GWIC-exposed male mice (scale bar = 100 µM). Insets show magnified views (scale bar = 50 µM). **(B)** Quantification of percent fraction GFAP+ cells within three regions of the hippocampus (DG, CA1, and CA3) in DMSO-exposed WT male mice and WT, NLRP3$^{-/-}$ and STING$^{gt/gt}$ GWIC-exposed male mice. (C) Tissue extracts were generated from microdissected hippocampi from DMSO-exposed WT, NLRP3$^{-/-}$ and STING$^{gt/gt}$ mice and immunoblotted for GFAP as described in Materials and Methods. Each lane represents one mouse, with N=3 for each genotype and sex. (D) Quantification of percent IBA-1+ cells with activated morphology in three hippocampal regions (CA1, CA3, and DG) in WT DMSO- and GWIC-exposed and NLRP3$^{-/-}$ and STING$^{gt/gt}$ GWIC-exposed male mice. Sections were scored blindly for total number of IBA-1+ cells and number of IBA-1+ cells with activated morphology; these values were then used to calculate percent fraction of IBA-1+ cells with activated morphology (number of IBA-1+ cells with activated morphology divided by total number of IBA-1+ cells). (B and D) Error bars represent the mean of biological replicates +/- SEM (N=5-6). Indicated p-values were calculated using two-tailed, unpaired, Student's t-test. *$p < 0.05$; $p<0.01$;***$p < 0.001$; **** $p < 0.0001$.